厚生労働科学研究難治性疾患克服事業

「難治性腸管吸収障害 Microscopic Colitis に関する調査研究」

平成 22 年度第 1 回総会プログラム

（敬称略）

平成22年7月30日（金）

開会（16：00）

Ⅰ．研究代表者挨拶（16：00～16：10）

渡辺　守（東京医科歯科大学大学院医歯学総合研究科消化器病態学）

Ⅱ．実態調査（16：10～16：30）

岡本隆一（東京医科歯科大学大学院医歯学総合研究科消化器病態学）

清水誠治（JR 大阪鉄道病院消化器内科）

Ⅲ．診断基準の作成に向けて～現状と問題点～（16：30～17：00）

臨床（16：30～16：40）

平田一郎（藤田保健衛生大学医学部消化管内科学）

内視鏡（16：40～16：50）

松井敏幸（福岡大学筑紫病院消化器科）

病理（16：50～17：00）

田中正則（弘前市立病院臨床検査科）

Ⅳ．治療指針の作成に向けて～現状と問題点～（17：00～17：10）

松本主之（九州大学大学院医学研究院病態機能内科学）

Ⅴ．病態の解明に向けて（17：10～17：30）

三浦総一郎（防衛医科大学校内科学）

岡本隆一／土屋輝一郎

（東京医科歯科大学大学院医歯学総合研究科消化器病態学）

閉会の挨拶

＜最終版＞

厚生労働科学研究難治性疾患克服研究事業
「難治性腸管吸収障害Microscopic Colitisに関する調査研究」
平成23年度第1回総会

期日　平成23年7月15日（金）14時30分～

場所　味の素㈱本社ビル（東京都中央区京橋1-15-1）

研究代表者　渡辺　守
（東京医科歯科大学消化器病態学）

事務局　東京医科歯科大学消化器病態学
担当　　岡本隆一
TEL：03-5803-5974　FAX：03-5803-0268
E-mail：rokamoto.gast@tmd.ac.jp

第１回総会について

１）演題発表について

(1) スライドは、Power Point で作成し、USB フラッシュメモリディスクまたは CD-ROM に保存したものをお持込み下さい。(Windows,Macintosh どちらも対応可能ですが、御自分の PC 以外の機器でも試写してからお持ち下さい。)

(2) B1 会場スライド受付までご提出下さい。その際、試写（出力確認）も必ず行ってください。使用したメディアは、画面確認後その場でご返却いたします。

(3) 発表・報告は３分でお願い致します。

２）発表データについて

厚生労働省への報告の必要上、発表スライドファイルを当日複製させていただきますことをご了承下さい。不都合のある先生におかれましては、事前に事務局まで御連絡お願いします。

３）会場セキュリティについて

(1) 一階玄関ホール総会受付にて芳名録へご署名後、セキュリティカードをお受け取りいただき、改札を通って地下一階会場へお進みください。

(2) 館内はセキュリティ制ですのでセキュリティカードを必ず常時携行してください。退出される際にはカードをご返却ください。カードの紛失があると全館内のセキュリティに支障を来たしますので、くれぐれも紛失ならびにお持ち帰りにならないようご注意ください。

４）駐車場について

駐車スペースはご用意しておりませんので、公共の交通機関をご利用ください。

５）会場案内図 味の素㈱本社ビル 東京都中央区京橋 1-15-1／℡ 03-5250-8111

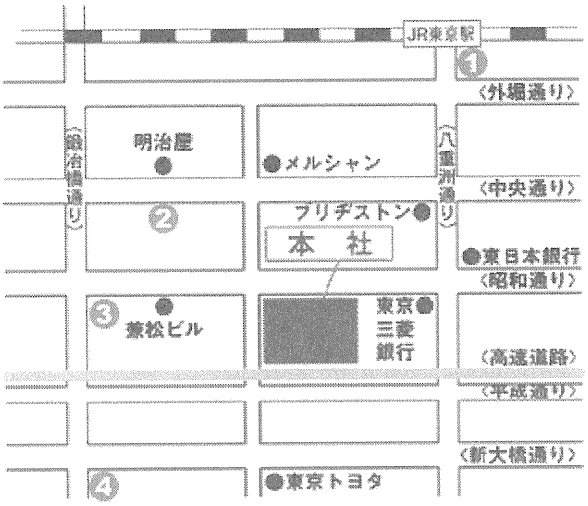

② 東京メトロ銀座線「京橋駅」６番出口（徒歩５分）

③ 都営浅草線「宝町駅」A-2 出口（徒歩３分）

④ 東京メトロ日比谷線「八丁堀駅」北口（徒歩 10 分）

厚生労働科学研究難治性疾患克服事業

「難治性腸管吸収障害 Microscopic Colitis に関する調査研究」

平成 23 年度第 1 回総会プログラム

（敬称略、発表予定者は○印）

平成23年7月15日（金）

開会（14：30）

Ⅰ．研究代表者挨拶（14：30～14：40）

渡辺　守（東京医科歯科大学大学院・消化器病態学）

Ⅱ．疾患概念と定義（14：40～14：55）

○平田一郎（藤田保健衛生大学・消化管内科学）

Ⅱ．実態調査（14：55～15：10）

○岡本隆一（東京医科歯科大学大学院・消化器病態学）

Ⅲ．診断基準の策定に向けて（15：10～15：40）

臨床診断

○松井敏幸（福岡大学筑紫病院・消化器内科）

清水誠治（JR 大阪鉄道病院・消化器内科）

病理診断

○原岡誠司（福岡大学筑紫病院・病理部）

○田中正則（弘前市立病院・臨床検査科）

Ⅳ．治療指針の策定に向けて（15：40～16：00）

○松本主之（九州大学大学院医学研究院・病態機能内科学）

緒方晴彦（慶應義塾大学医学部・内視鏡センター）

Ⅴ．病態の解明に向けて（16：00～16：20）

○三浦総一郎（防衛医科大学校・内科学）

○土屋輝一郎（東京医科歯科大学大学院・消化器病態学）

○ 佐藤俊朗[1]、緒方晴彦[2]、日比紀文[1]

（慶応義塾大学医学部・消化器内科[1]、同 内視鏡センター[2]）

閉会の挨拶（16：30 終了予定）

Ⅶ.　研究成果の別刷り

nature medicine

Functional engraftment of colon epithelium expanded *in vitro* from a single adult Lgr5$^+$ stem cell

Shiro Yui[1,6], Tetsuya Nakamura[2,6], Toshiro Sato[3,5], Yasuhiro Nemoto[1], Tomohiro Mizutani[1], Xiu Zheng[1], Shizuko Ichinose[4], Takashi Nagaishi[1], Ryuichi Okamoto[2], Kiichiro Tsuchiya[1], Hans Clevers[3] & Mamoru Watanabe[1]

Adult stem-cell therapy holds promise for the treatment of gastrointestinal diseases. Here we describe methods for long-term expansion of colonic stem cells positive for leucine-rich repeat containing G protein-coupled receptor 5 (Lgr5$^+$ cells) in culture. To test the transplantability of these cells, we reintroduced cultured GFP$^+$ colon organoids into superficially damaged mouse colon. The transplanted donor cells readily integrated into the mouse colon, covering the area that lacked epithelium as a result of the introduced damage in recipient mice. At 4 weeks after transplantation, the donor-derived cells constituted a single-layered epithelium, which formed self-renewing crypts that were functionally and histologically normal. Moreover, we observed long-term (>6 months) engraftment with transplantation of organoids derived from a single Lgr5$^+$ colon stem cell after extensive *in vitro* expansion. These data show the feasibility of colon stem-cell therapy based on the *in vitro* expansion of a single adult colonic stem cell.

Epithelial stem cells maintain tissue homeostasis throughout the gastrointestinal tract[1–3]. The Wnt, bone morphogenetic protein (BMP) and Notch cascades function together to regulate stem-cell maintenance[4,5]. *Lgr5* marks stem cells in small intestinal and colonic crypts[6] and in gastric units[7]. *Bmi1* may mark distinct stem cells in the proximal small intestine[8]. It has been shown that freshly isolated intestinal epithelium can be transplanted in rodents after resident epithelium has been surgically removed[9,10]. We previously developed a three-dimensional culture technique that allows expansion of single Lgr5$^+$ stem cells from small intestine[11], stomach[7] and colon[12]. The resulting organoids then expand and self organize into an epithelial architecture that is reminiscent of that seen in *in vivo* histology. Moreover, the growing organoids maintain their tissue identity even after prolonged culture. Here we sought to evaluate whether the cultured Lgr5$^+$ cells faithfully represent the tissue-resident Lgr5$^+$ stem cells and, thus, are able to regenerate epithelial tissue *in vivo*. Considering that the colon is very vulnerable to disease in humans, we focused on colonic stem cells in our analyses.

RESULTS

Long-term, serum-free culture system for colonic organoids

We subjected the colons of adult mice to a combination of enzymes[13], reducing agents[14] and mechanical disruption. The resulting crypt fragments were mostly devoid of α smooth muscle actin gene (*Acta2*)-expression–positive non-epithelial components and consisted of a mix of cadherin 1, type 1, E-cadherin (*Cdh1*)$^+$ cells expressing terminal differentiation marker genes (*Muc2*, *CA2* and *ChgA*) and Lgr5$^+$ stem cells (**Supplementary Fig. 1a,b**).

The addition of R-spondin 1 (Rspo1), Noggin and epidermal growth factor (EGF), which are all essential to small intestine culture[11], did not maintain the growth of colonic crypts. We therefore developed the following 'TMDU (Tokyo Medical and Dental University) protocol': we embedded crypts in type I collagen in serum-free medium with Wnt3a, hepatocyte growth factor (HGF)[15,16] and BSA, in addition to Rspo1, Noggin and EGF (**Supplementary Fig. 1c**). Sequential imaging of the cultures revealed rapid growth of cystic structures (**Fig. 1a**). Wnt3a, Rspo1 and BSA were essential to this growth (**Supplementary Fig. 1d**). As predicted by previous results[17,18], Rspo1 could be substituted with Wnt3a (data not shown). Although Noggin, EGF and HGF were not essential for growth of the colonic crypts, each enhanced their growth (**Supplementary Fig. 1e**). The colonic organoids rarely had buds (**Fig. 1a**, **Supplementary Fig. 2a** and **Supplementary Video 1**). Of note, small intestinal organoids also generate cystic structures when Wnt3a is added to them[19].

The colonic organoids were single layered (**Supplementary Fig. 2b**), and all the cells within were positive for Cdh1 expression (**Fig. 1b**). The basal membranes of the organoids faced outward (**Fig. 1b**). Ki67$^+$ cells were present in the colonic organoids (**Fig. 1b**), as were alcian blue–positive goblet cells, chromogranin A (ChgA)$^+$ enteroendocrine cells, carbonic anhydrase II (CA2)$^+$ colonocytes and cytochrome c oxidase subunit I (COX1)$^+$ tuft cells[20] (**Fig. 1b**). Transmission electron microscopy revealed epithelial characteristics such as microvilli (**Fig. 1c**) and junctional complexes (**Fig. 1d**) in the organoids. However, stromal cells were absent (**Supplementary Fig. 2c**). Mitotic cells with condensed chromosomes were present in the organoids (**Fig. 1e**), and goblet cells (**Fig. 1f**) and enteroendocrine cells (**Fig. 1g**) could also be clearly detected.

[1]Department of Gastroenterology and Hepatology, Graduate School, Tokyo Medical and Dental University, Bunkyo-ku, Tokyo, Japan. [2]Department of Advanced Therapeutics for Gastrointestinal Diseases, Tokyo Medical and Dental University, Bunkyo-ku, Tokyo, Japan. [3]Hubrecht Institute and University Medical Centre, Utrecht, The Netherlands. [4]Research Center for Medical and Dental Sciences, Tokyo Medical and Dental University, Bunkyo-ku, Tokyo, Japan. [5]Present address: Department of Gastroenterology, Keio University School of Medicine, Shinjuku-ku, Tokyo, Japan. [6]These authors contributed equally to this work. Correspondence should be addressed to H.C. (h.clevers@hubrecht.eu) or M.W. (mamoru.gast@tmd.ac.jp).

Received 30 July 2011; accepted 29 November 2011; published online 11 March 2012; doi:10.1038/nm.2695

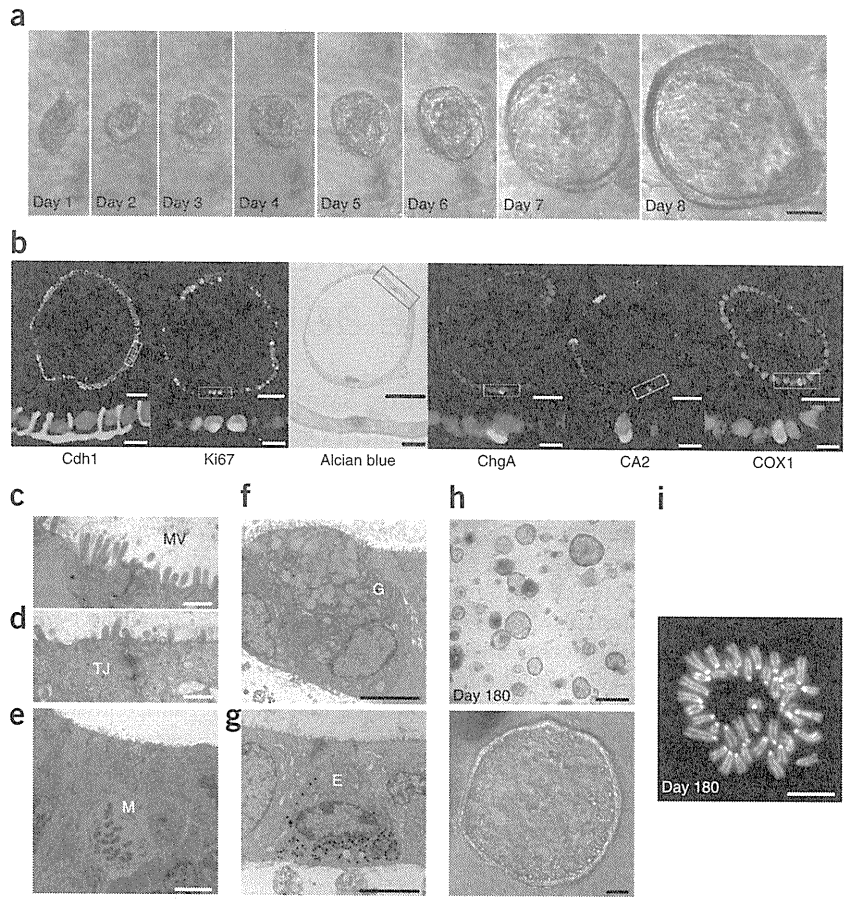

Figure 1 Long-term, serum-free culture of colonic epithelial cells. (**a**) A representative colonic crypt growing as a cystic structure. Scale bar, 50 μm. Time-lapse images of another colonic crypt are shown in **Supplementary Figure 2a** and **Supplementary Video 1**. (**b**) Histology of the colonic organoids at day 8 of culture. Cdh1$^+$ cells, actively proliferating Ki67$^+$ cells (green) and terminally differentiated cells stained with alcian blue (blue, goblet cells) or immunostained with ChgA (green, enteroendocrine cells), CA2 (green, colonocytes) or COX1 (green, tuft cells) are shown. Higher magnification views of the boxed areas are shown at the bottom. DAPI staining was performed, except for the experiments in which we performed alcian blue staining. Scale bars, top, 50 μm; bottom, 10 μm. (**c–g**) Transmission electron microscopy analysis for organoids at day 8. (**c**,**d**) Microvilli (MV) and intracellular tight junctions (TJ) are shown. (**e**) Mitotic (M) cells showing chromatin condensation. (**f**,**g**) Goblet cells (G) with mucus granules (**f**) and enteroendocrine cells (E) with electron dense granules (**g**) are shown. Scale bars: **c**,**d**, 0.5 μm; **e–g**, 5 μm. Low-power views of **f** and **g** are also shown in **Supplementary Figure 2c**. (**h**) The culture at day 180 (top) and its representative organoid (bottom). Scale bars, top, 500 μm; bottom, 50 μm. Images of the growth of a single cell after passage are shown in **Supplementary Figure 3** and **Supplementary Video 2**. (**i**) Metaphase spread of a cell at day 180 shows a normal karyotype ($2n = 40$). Scale bar, 10 μm.

The organoids could be passaged weekly at a 1:2 ratio (**Supplementary Fig. 3** and **Supplementary Video 2**). Addition of the Rho kinase inhibitor Y-27632 (ref. 21) improved the replating efficiency of the organoids[11]. We successfully propagated organoids for more than 6 months without clear alterations of morphology (**Fig. 1h**) or karyotype (**Fig. 1i**).

Lgr5$^+$ cells are enriched in colonic organoids

We tracked the expression of *Lgr5* over 60 d and found a substantial elevation during the first 8 d of observation (**Fig. 2a**). We found no change in the expression of *ChgA* and *CA2*, whereas *Muc2* expression was repressed in the first 8 d (**Fig. 2a**). Addition of a combination of Wnt3a, Rspo1 and BSA induced *Lgr5* expression (**Fig. 2b**). *Lgr5* expression was further upregulated by the addition of Noggin, which is an antagonist of BMP[22] (**Fig. 2b**). The Notch pathway suppresses the

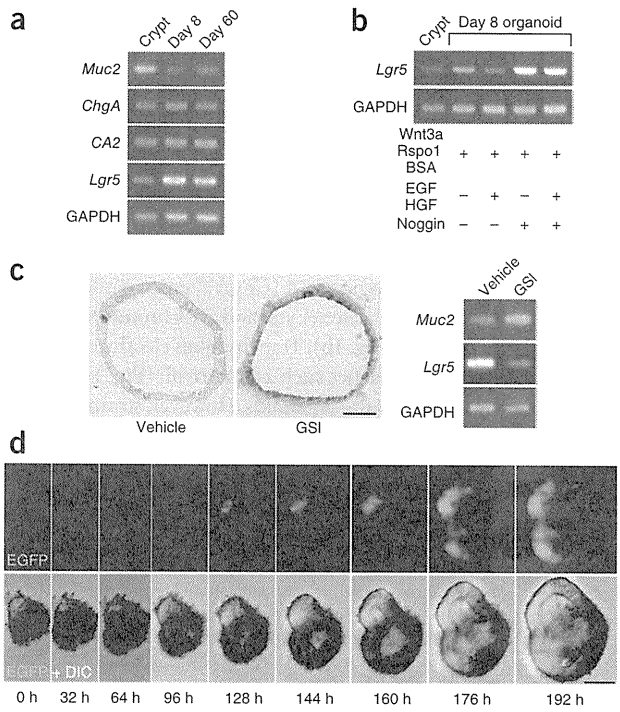

Figure 2 Lgr5$^+$ stem cells are enriched in cultured organoids. (**a**) RT-PCR analysis of the colonic crypts immediately after isolation (crypt) or organoids cultured for 8 or 60 d. *Lgr5* was upregulated and stayed constant thereafter. Differentiation marker genes (*Muc2*, *ChgA* and *CA2*) were expressed over 60 d. The primers used are listed in **Supplementary Table 1**. (**b**) RT-PCR shows that *Lgr5* upregulation is mediated by a combination of minimum factors (Wnt3a, Rspo1 and BSA) and Noggin but not by EGF and HGF. (**c**) Notch signal-mediated cell fate determination *in vitro*. Cultured organoids were treated with GSI, LY-411575 or vehicle alone from day 4 to day 8. Organoids stained with alcian blue are shown (left). Scale bar, 50 μm. RT-PCR shows that the expression of *Muc2* is upregulated, whereas the expression of *Lgr5* is reciprocally downregulated in organoids treated with LY-411575 (GSI, right). Similar results were obtained in three independent experiments, and representative data are shown. (**d**) A time-lapse imaging of a growing colonic crypt obtained from an *Lgr5-EGFP-ires-CreERT2* mouse over 192 h. The top panel shows EGFP and the bottom panel shows merged images of EGFP and differential interference contrast (DIC). Scale bar, 50 μm. The corresponding video (**Supplementary Video 3**) and similar results from another example are available as **Supplementary Figure 4a** and **Supplementary Video 4**.

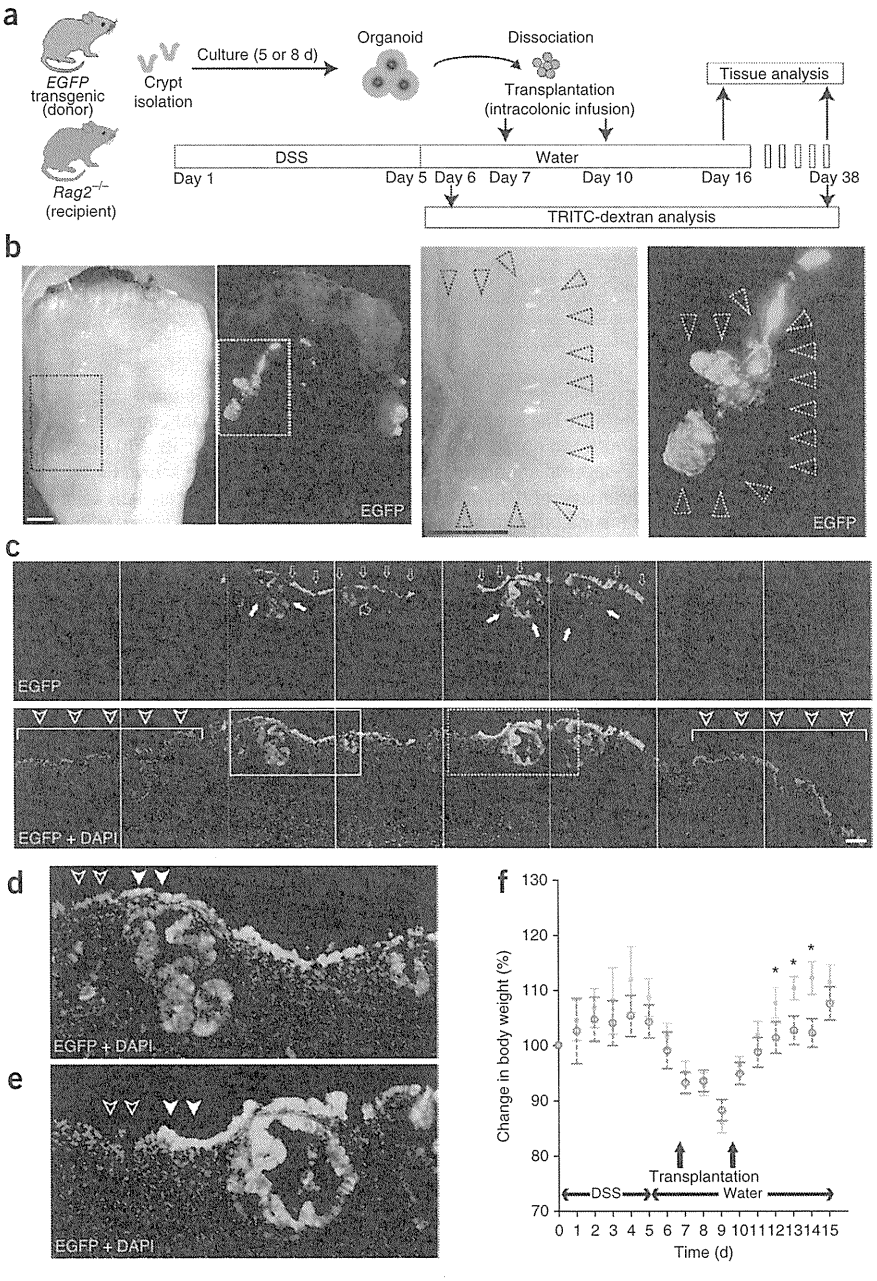

Figure 3 Transplantation of cultured cells improves acute colitis. (**a**) Experimental protocols. (**b**) Recipient colon at 6 d after transplantation. Low-power views (stereoscopic and fluorescent images) are shown on the left. High-power views of the areas in the dotted squares are shown in the right. The black dotted arrowheads show a depressed area surrounded by edematous mucosa. EGFP$^+$ areas overlapping the damaged region (white dotted arrowheads) are also shown. Note that the outline of the tissue is not precisely the same in the stereoscopic and fluorescent images, as they were acquired on different microscopes. Scale bars, 1 mm. (**c**) Histology of the EGFP$^+$ area shown in **b**. EGFP (top) and the merged image with DAPI staining (bottom). EGFP$^+$ cells cover the damaged mucosa that intervene separate areas preserving crypt structures (bottom, arrowheads). EGFP$^+$ cells constitute flat linings (top, narrow open arrow) or an invagination (top, wide open arrows), the latter of which is reminiscent of crypts. EGFP$^+$ cystic structures were also observed in the EGFP$^+$ cells (top, filled white arrows). The regions in the solid- and dotted-line boxes are shown at higher magnification in **d** and **e**, respectively. Scale bar, 100 μm. (**d**) High-power view of the solid box in **c**. (**e**) High-power view of the dotted box in **c**. (**f**) *Rag2*$^{-/-}$ mice were given DSS for 5 d, and then transplantation ($n = 6$) or sham-transplantion ($n = 6$) was performed. On day 16, the presence of engraftment was retrospectively assessed after the mice were killed. The body weights of the mice with EGFP$^+$ engraftment (green squares, $n = 4$) and sham-transplanted controls (red open circles, $n = 6$) are presented as a percentage of their initial weight. Error bars, s.e.m. $^*P < 0.05$ (Student's t test).

differentiation of progenitors[23,24] and stem cells[25] toward secretory lineages. We treated the colonic organoids with LY-411575, a γ-secretase inhibitor (GSI) that is capable of inhibiting Notch signaling[26,27]. Notch inhibition induced a goblet-cell phenotype with an increased level of *Muc2* mRNA and a reciprocal decrease in the expression of *Lgr5* (**Fig. 2c**).

We next performed live imaging of colonic organoids obtained from *Lgr5-EGFP-internal ribosome entry site (ires)-CreERT2* mice[6] in which an enhanced GFP (EGFP) and tamoxifen-inducible Cre recombinase cassette is integrated into the *Lgr5* locus. The *Lgr5*-promoter–driven EGFP expression initially stayed at a marginal level but then increased beginning at day 5 (**Fig. 2d**, **Supplementary Fig. 4a** and **Supplementary Videos 3** and **4**). We confirmed the expansion of Lgr5$^+$ cells at a single-cell resolution (**Supplementary Fig. 4b**). Over multiple passages, the *Lgr5-EGFP* locus tended to become silenced, whereas the wild-type *Lgr5* allele remained active (**Fig. 2a,b**). Taken together, colonic Lgr5$^+$ stem cells were able to self renew and expand *in vitro*.

Cultured colonic organoids rescue damaged epithelium

We next tested the transplantability of the cultured organoids (**Fig. 3a**). We induced colonic mucosal damage by providing immunocompromised *Rag2*$^{-/-}$ mice with colitis-inducing dextran sulfate sodium (DSS)[28] for 5 d. Most of the mice developed acute colitis characterized by weight loss, bloody stool, diarrhea and epithelial injury in the distal colon. At 7 and 10 d after initiating DSS administration, we dissociated the organoids cultured from *EGFP* transgenic mice[29] into small fragments, suspended them in a Matrigel-containing PBS and instilled them by enema in recipient mice.

At 16 d after the start of DSS administration, the recipient colons showed varying degrees of recovery. Multiple EGFP$^+$ areas appeared as well-demarcated patches in the treated colons (**Fig. 3b**). We did not observe any EGFP$^+$ areas in colons not treated with DSS (data not shown). Histologically, the EGFP$^+$ cells covered the submucosa and were located between the less damaged recipient tissues (**Fig. 3c**). The EGFP$^+$ cells formed flat or slightly invaginated linings (**Fig. 3c**). We also observed large cystic EGFP$^+$ structures below the surface of the treated colons (**Fig. 3c**). Some of the EGFP$^+$ areas connected to the recipients' epithelium (**Fig. 3d**), whereas others repopulated areas that were devoid of recipient epithelium (**Fig. 3e**). Notably, the body weights of the mice with engraftment were

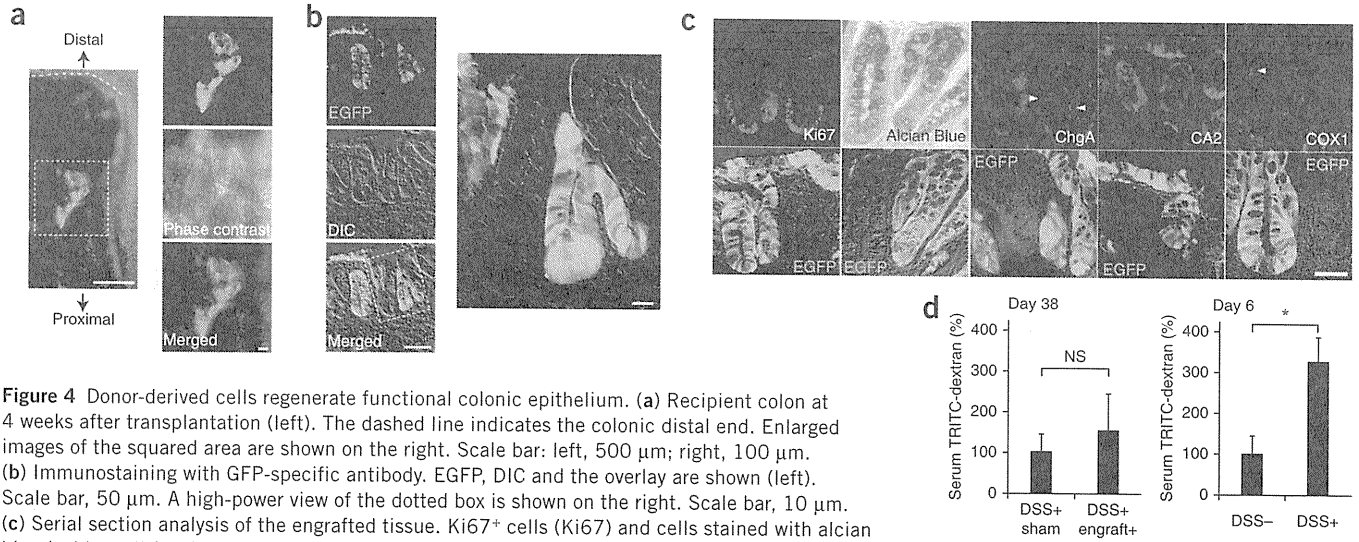

Figure 4 Donor-derived cells regenerate functional colonic epithelium. (**a**) Recipient colon at 4 weeks after transplantation (left). The dashed line indicates the colonic distal end. Enlarged images of the squared area are shown on the right. Scale bar: left, 500 μm; right, 100 μm. (**b**) Immunostaining with GFP-specific antibody. EGFP, DIC and the overlay are shown (left). Scale bar, 50 μm. A high-power view of the dotted box is shown on the right. Scale bar, 10 μm. (**c**) Serial section analysis of the engrafted tissue. Ki67$^+$ cells (Ki67) and cells stained with alcian blue (goblet cells) or immunostained for ChgA, CA2 and COX1 are shown. Images are shown with or without DAPI staining. The bottom row shows neighboring sections stained for GFP. Arrowheads point to ChgA$^+$ or COX1$^+$ cells. Scale bar, 50 μm. (**d**) After DSS colitis induction, transplantation ($n = 6$) or sham transplantation ($n = 6$) was performed. Mice were administered TRITC-dextran by gavage before killing on day 38. Four out of six colons in the transplanted group had EGFP$^+$ engraftment, and the serum TRITC concentration in these mice is shown (DSS+ engraft+; $n = 4$) as a percentage of that in the sham-transplanted group (DSS+ sham; $n = 6$). As a control, DSS colitis was induced (DSS+; $n = 6$) or uninduced (DSS–; $n = 6$) in *Rag2*$^{-/-}$ mice, and these mice were subjected for the same assay on day 6 without transplantation. Data are shown as a percentage of the concentrations in uninduced mice. Error bars, s.e.m. $^*P < 0.05$, NS, not significant (Student's *t* test).

higher than those of sham-transplanted mice (**Fig. 3f**; with statistically significant results at days 12, 13 and 14, $P < 0.05$).

At 4 weeks after transplantation, tube-like EGFP$^+$ crypts appeared in the distal colon (**Fig. 4a**) that were morphologically indistinguishable from the surrounding EGFP$^-$ epithelium (**Fig. 4b**). Notably, the engrafted crypts were entirely EGFP$^+$, indicating the presence of EGFP$^+$ stem cells (**Fig. 4b**). Cells in the lower part of the EGFP$^+$ crypts were normally Ki67$^+$, and the EGFP$^+$ crypts contained all

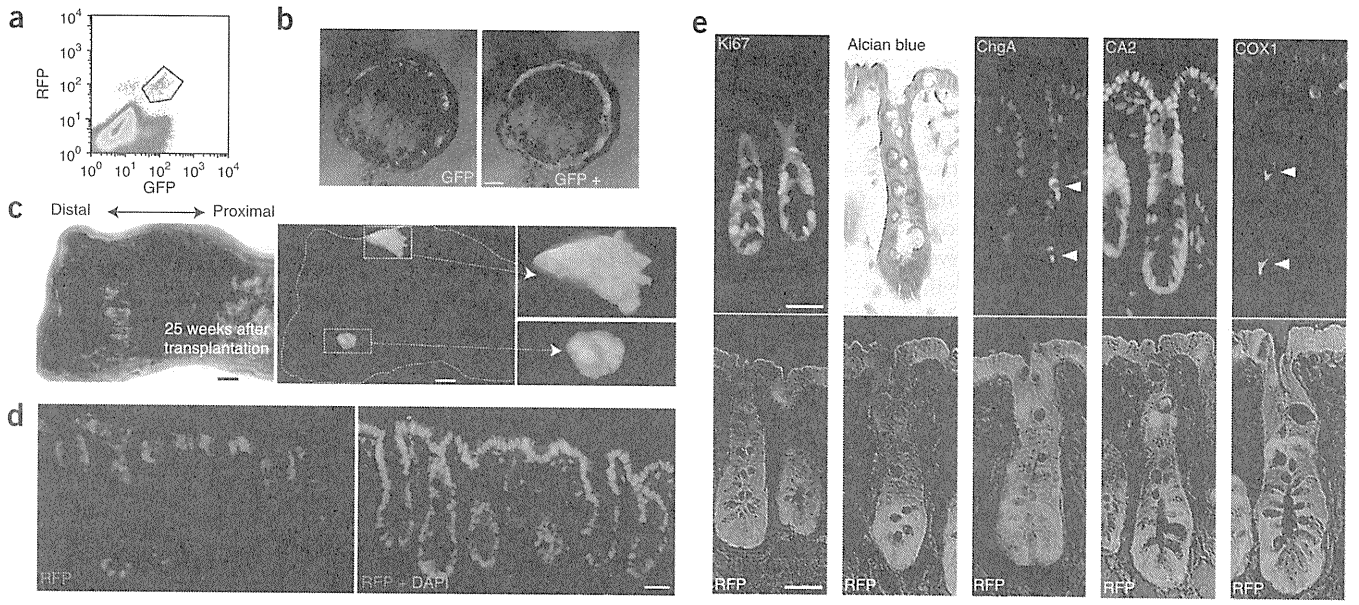

Figure 5 Single Lgr5$^+$ stem-cell–derived cultured cells serve as long-lived, multipotential stem cells *in vivo*. (**a**) Fluorescence-activated cell sorting analysis of colonic cells of *R26R-Confetti* mice crossed with *Lgr5-EGFP-ires-CreERT2* mice 3 d after Cre induction. The EGFP$^+$ and RFP$^+$ populations located in the box were sorted and cultured. (**b**) Images are shown of one out of four organoids grown from sorted single Lgr5$^+$ cells at day 6. EGFP$^+$ stem cells are scattered in the organoid (left), with all the offspring being positive for RFP (right). Scale bar, 50 μm. (**c**) Images of the recipient colon at 25 weeks after transplantation. The phase-contrast view of the recipient colon is shown on the left. The fluorescent image shows the tissue contains RFP$^+$ grafts (right). Scale bar, 1 mm. Enlarged images of the boxed areas are also shown (2.7-fold magnification). (**d**) Immunostaining of the RFP$^+$ engraft at 25 weeks after transplantation. An image of RFP-specific antibody staining (left) and an image of RFP staining merged with DAPI staining (right) are shown. Scale bar, 50 μm. (**e**) Serial section analysis of the engrafted RFP$^+$ tissue at 25 weeks after transplantation. The top panels show Ki67, alcian blue, ChgA, CA2 or COX1 staining with or without nuclei stained by DAPI. The bottom panels show the adjacent sections stained for RFP. Arrowheads point to ChgA$^+$ enteroendocrine cells and COX1$^+$ tuft cells. Scale bars, 50 μm.

terminally differentiated cell types (**Fig. 4c**). We probed the epithelial permeability of the engrafts using tetramethylrhodamine isothiocyanate (TRITC)-conjugated dextran (TRITC-dextran). Blood TRITC concentrations in transplanted mice were comparable to those in control mice, indicating a maintenance of epithelial barrier function in these engrafts (**Fig. 4d**). Notably, transplantation was less successful with freshly isolated donor cells ($P < 0.05$, Mann-Whitney U test; **Supplementary Fig. 5**), suggesting that the expansion of stem cells during the culture is associated with a higher success rate of transplantation. In addition, Matrigel-containing organoid suspensions transplanted better than organoids suspended in PBS (**Supplementary Fig. 5**; $P < 0.05$, Mann-Whitney U test), proposing a role for the simultaneous supply of extracellular matrix in successful transplantation.

Engraftment of organoids derived from a single Lgr5$^+$ cell

We next sought to initiate the protocol described above from a single stem cell (**Supplementary Fig. 6a**). We crossed *Lgr5-EGFP-ires-CreERT2* mice with *R26R-Confetti* reporter mice[30]. In the resulting offspring, tamoxifen-induced Cre activation resulted in Cre-mediated recombination at the *Rosa26* locus in individual Lgr5$^+$ stem cells, leading to stochastically selected expression of one out of four fluorescent proteins: red fluorescent protein (RFP), cyan fluorescent protein (CFP), GFP or yellow fluorescent protein (YFP). At 3 d after Cre activation, we sorted cells double positive for Lgr5-EGFP and Confetti-RFP, which consisted of ~0.02% of the total cells (**Fig. 5a**), equivalent to ~100 cells per mouse.

We cultured the sorted cells after a limiting dilution (100 cells per 96 well) using the Hubrecht protocol (Online Methods; protocol described previously[12] with addition of Y-27632 in the first 2 d). Four stem cells double positive for Lgr5-EGFP and Confetti-RFP grew out, which was comparable to the culture efficiency of small intestinal stem cells[11] (**Fig. 5b**). Organoids were expanded to more than 100 wells in >10 weeks, frozen and shipped. After thawing, we recovered the cells under the TMDU protocol. We transplanted ~500 organoids per recipient mouse, as described above. Analyses at 4, 17, 21 and 25 weeks after transplantation revealed the presence of grafts in these mice (**Fig. 5c** and **Supplementary Figs. 6b,c** and **7a**). At 25 weeks after transplantation, RFP$^+$ cells still generated a single-layered epithelium. We noted no sign of adenomatous or dysplastic change in any of the transplanted areas (**Fig. 5d**). Again, all differentiated cell types, as well as Ki67$^+$ proliferating cells, were present at normal ratios (**Fig. 5e** and **Supplementary Fig. 7b**).

DISCUSSION

Here we describe methodologies to isolate, culture and transplant Lgr5$^+$ colon stem cells. Our observations confirm that *Lgr5* marks genuine stem cells that retain their self-renewal and multilineage-differentiation properties even after prolonged culture. A major difference between small-intestinal and colon-culture conditions is in the latter's requirement for Wnt. Although Wnt factors can initiate Wnt signals on their own, R-spondins (such as Rspo1) can only augment preexisting Wnt signals[31]. Because Paneth cells produce Wnt3, they serve as the center of organization of the stem cell niche[19]. At the colon crypt bottoms, secretory cells are located between the Lgr5$^+$ stem cells that—like Paneth cells—express CD24 (ref. 19). However, these CD24$^+$ secretory cells do not produce a sufficient amount of Wnt proteins *in vitro* (data not shown). Therefore, colon organoids cannot grow from Rspo1 alone but, rather, also require exogenous Wnt.

This study provides proof of principle that cultured Lgr5$^+$ cells can be used for stem-cell therapy to repair damaged epithelium. Transplanted cells adhere to and cover superficially damaged tissue. Further, engrafted recipient mice had higher body weights than ungrafted controls, implying a beneficial role for the donor cells in DSS-induced acute colitis. Although further optimization is clearly needed, the current study implies that *in vitro* expansion and transplantation of gastrointestinal stem cells may be a promising option for patients with severe gastrointestinal epithelial injuries.

Lgr5$^+$ stem cells divide once every day *in vivo*[6], thus defying the Hayflick limit[32]. They appear similarly unrestricted in their proliferative capacity *in vitro*, while they retain their original tissue identity. It is of interest that the Lgr5 protein is now known to reside in the Wnt receptor complex to function as a receptor for Rspo1 (refs. 33,34), which is a crucial component of long-term organoid culture systems that we have developed. As the resulting organoids have now been proven to be transplantable, the Lgr5$^+$ stem cell isolation and expansion technology may provide a simple and safe avenue for the development of new regenerative and gene-therapy strategies.

METHODS

Methods and any associated references are available in the online version of the paper at http://www.nature.com/naturemedicine/.

Note: Supplementary information is available on the Nature Medicine website.

ACKNOWLEDGMENTS

We thank M. Okabe (Osaka University) for EGFP transgenic mice and Y. Kato, J. Inazawa, I. Sekiya (TMDU), H. Snippert and R. Vries (Hubrecht Institute) for technical assistance. This study was supported by Grant-in-Aid for Scientific Research from the Japanese Ministry of Education, Culture, Sports, Science and Technology, by the Health and Labour Sciences Research Grants for Research on Intractable Diseases from Ministry of Health, Labour and Welfare of Japan, and by a grant from the European Research Council and from the Dutch Cancer Foundation.

AUTHOR CONTRIBUTIONS

T. Nakamura, H.C. and M.W. designed the study. S.Y., T. Nakamura and T.S. performed experiments and analyzed data. T. Nakamura, T.S. and H.C. wrote the paper. Y.N., T. Nagaishi and K.T. assisted in transplantation experiments. T.M., X.Z. and K.T. gave support in gene analysis. R.O. helped with the immunohistochemistry. S.I. advised on the electron microscopy. H.C. and M.W. gave conceptual advice and supervised the project.

COMPETING FINANCIAL INTERESTS

The authors declare competing financial interests: details accompany the full-text HTML version of the paper at http://www.nature.com/naturemedicine/.

Published online at http://www.nature.com/naturemedicine/.
Reprints and permissions information is available online at http://www.nature.com/reprints/index.html.

1. Potten, C.S., Booth, C. & Pritchard, D.M. The intestinal epithelial stem cell: the mucosal governor. *Int. J. Exp. Pathol.* **78**, 219–243 (1997).
2. Bjerknes, M. & Cheng, H. Intestinal epithelial stem cells and progenitors. *Methods Enzymol.* **419**, 337–383 (2006).
3. Barker, N., van de Wetering, M. & Clevers, H. The intestinal stem cell. *Genes Dev.* **22**, 1856–1864 (2008).
4. Crosnier, C., Stamataki, D. & Lewis, J. Organizing cell renewal in the intestine: stem cells, signals and combinatorial control. *Nat. Rev. Genet.* **7**, 349–359 (2006).
5. Radtke, F. & Clevers, H. Self-renewal and cancer of the gut: two sides of a coin. *Science* **307**, 1904–1909 (2005).
6. Barker, N. *et al.* Identification of stem cells in small intestine and colon by marker gene *Lgr5*. *Nature* **449**, 1003–1007 (2007).
7. Barker, N. *et al.* Lgr5^{+ve} stem cells drive self-renewal in the stomach and build long-lived gastric units *in vitro*. *Cell Stem Cell* **6**, 25–36 (2010).
8. Sangiorgi, E. & Capecchi, M.R. *Bmi1* is expressed *in vivo* in intestinal stem cells. *Nat. Genet.* **40**, 915–920 (2008).
9. Avansino, J.R., Chen, D.C., Woolman, J.D., Hoagland, V.D. & Stelzner, M. Engraftment of mucosal stem cells into murine jejunum is dependent on optimal dose of cells. *J. Surg. Res.* **132**, 74–79 (2006).
10. Tait, I.S., Evans, G.S., Flint, N. & Campbell, F.C. Colonic mucosal replacement by syngeneic small intestinal stem cell transplantation. *Am. J. Surg.* **167**, 67–72 (1994).

11. Sato, T. *et al.* Single Lgr5 stem cells build crypt-villus structures *in vitro* without a mesenchymal niche. *Nature* **459**, 262–265 (2009).
12. Sato, T. *et al.* Long-term expansion of epithelial organoids from human colon, adenoma, adenocarcinoma, and Barrett's epithelium. *Gastroenterology* **141**, 1762–1772 (2011).
13. Booth, C., Patel, S., Bennion, G.R. & Potten, C.S. The isolation and culture of adult mouse colonic epithelium. *Epithelial Cell Biol.* **4**, 76–86 (1995).
14. Whitehead, R.H., Demmler, K., Rockman, S.P. & Watson, N.K. Clonogenic growth of epithelial cells from normal colonic mucosa from both mice and humans. *Gastroenterology* **117**, 858–865 (1999).
15. Kanayama, M. *et al.* Hepatocyte growth factor promotes colonic epithelial regeneration via Akt signaling. *Am. J. Physiol. Gastrointest. Liver Physiol.* **293**, G230–G239 (2007).
16. Tahara, Y. *et al.* Hepatocyte growth factor facilitates colonic mucosal repair in experimental ulcerative colitis in rats. *J. Pharmacol. Exp. Ther.* **307**, 146–151 (2003).
17. Kim, K.A. *et al.* Mitogenic influence of human R-spondin1 on the intestinal epithelium. *Science* **309**, 1256–1259 (2005).
18. Wei, Q. *et al.* R-spondin1 is a high affinity ligand for LRP6 and induces LRP6 phosphorylation and β-catenin signaling. *J. Biol. Chem.* **282**, 15903–15911 (2007).
19. Sato, T. *et al.* Paneth cells constitute the niche for Lgr5 stem cells in intestinal crypts. *Nature* **469**, 415–418 (2011).
20. Gerbe, F. *et al.* Distinct ATOH1 and Neurog3 requirements define tuft cells as a new secretory cell type in the intestinal epithelium. *J. Cell Biol.* **192**, 767–780 (2011).
21. Watanabe, K. *et al.* A ROCK inhibitor permits survival of dissociated human embryonic stem cells. *Nat. Biotechnol.* **25**, 681–686 (2007).
22. Haramis, A.P. *et al. De novo* crypt formation and juvenile polyposis on BMP inhibition in mouse intestine. *Science* **303**, 1684–1686 (2004).
23. Fre, S. *et al.* Notch signals control the fate of immature progenitor cells in the intestine. *Nature* **435**, 964–968 (2005).
24. van Es, J.H. *et al.* Notch/γ-secretase inhibition turns proliferative cells in intestinal crypts and adenomas into goblet cells. *Nature* **435**, 959–963 (2005).
25. van Es, J.H., de Geest, N., van de Born, M., Clevers, H. & Hassan, B.A. Intestinal stem cells lacking the Math1 tumour suppressor are refractory to Notch inhibitors. *Nat. Commun.* **1**, 18 (2010).
26. Wong, G.T. *et al.* Chronic treatment with the γ-secretase inhibitor LY-411,575 inhibits β-amyloid peptide production and alters lymphopoiesis and intestinal cell differentiation. *J. Biol. Chem.* **279**, 12876–12882 (2004).
27. Okamoto, R. *et al.* Requirement of Notch activation during regeneration of the intestinal epithelia. *Am. J. Physiol. Gastrointest. Liver Physiol.* **296**, G23–G35 (2009).
28. Wirtz, S., Neufert, C., Weigmann, B. & Neurath, M.F. Chemically induced mouse models of intestinal inflammation. *Nat. Protoc.* **2**, 541–546 (2007).
29. Okabe, M., Ikawa, M., Kominami, K., Nakanishi, T. & Nishimune, Y. 'Green mice' as a source of ubiquitous green cells. *FEBS Lett.* **407**, 313–319 (1997).
30. Snippert, H.J. *et al.* Intestinal crypt homeostasis results from neutral competition between symmetrically dividing Lgr5 stem cells. *Cell* **143**, 134–144 (2010).
31. Binnerts, M.E. *et al.* R-Spondin1 regulates Wnt signaling by inhibiting internalization of LRP6. *Proc. Natl. Acad. Sci. USA* **104**, 14700–14705 (2007).
32. Hayflick, L. & Moorhead, P.S. The serial cultivation of human diploid cell strains. *Exp. Cell Res.* **25**, 585–621 (1961).
33. de Lau, W. *et al.* Lgr5 homologues associate with Wnt receptors and mediate R-spondin signalling. *Nature* **476**, 293–297 (2011).
34. Carmon, K.S., Gong, X., Lin, Q., Thomas, A. & Liu, Q. R-spondins function as ligands of the orphan receptors LGR4 and LGR5 to regulate Wnt/β-catenin signaling. *Proc. Natl. Acad. Sci. USA* **108**, 11452–11457 (2011).

ONLINE METHODS

Mice. *Rag2*$^{-/-}$ mice were from Taconic Farms and Central Laboratories for Experimental Animals. *EGFP* transgenic mice[29], *Lgr5-EGFP-ires-CreERT2* mice[6] and *R26R-Confetti* mice[30] are described elsewhere. Male and female mice were randomly used for all experiments. All animal experiments were performed with the approval of the Institutional Animal Care and Use Committee of TMDU.

TMDU protocol for crypt isolation and three-dimensional culture. The colonic tissue was minced and digested. The crypts were further purified by mechanical disruption and density gradient centrifugation. A total of 2,000 crypts were suspended in 200 μl of the collagen type I solution (Nitta Gelatin Inc.) and placed in 48-well plates. After polymerization, 500 μl of Advanced DMEM/F12 containing BSA (Sigma), mouse EGF (mEGF) (PeproTech), mWnt3a, mRspo1, mHGF and mNoggin (all from R&D Systems) was added (TMDU medium). For passage, the gel was digested, and then the organoids were disaggregated with EDTA. The dissociated organoids were mixed in type I collagen solution and used for culture. A Rho kinase inhibitor, Y-27632, was added for the first 2 d after the cells were propagated. Where indicated, to induce goblet cell differentiation, organoids were treated with LY-411575, a GSI. See details in the **Supplementary Methods**.

Chromosome analysis. Chromosome karyotyping was performed according to a standard protocol as detailed in the **Supplementary Methods**.

Stereomicroscopy, phase-contrast imaging and histology. Images were acquired on either a fluorescence microscope equipped with phase-contrast setting (BZ-8000, KEYENCE), a fluorescent stereomicroscope system MVX10 (Olympus) or a fluorescence microscope DeltaVision system (Applied Precision). For histology and immunohistochemistry, tissues and organoids were fixed, sequentially dehydrated in sucrose in PBS, and frozen in OCT compound (Tissue Tek). Cryosections were examined by conventional H&E, alcian blue staining and a spectrum of immunohistochemical reactions, as detailed in the **Supplementary Methods**.

Transmission electron microscopy. Transmission electron microscopy was performed in a standard fashion and is detailed in the **Supplementary Methods**.

Live imaging. Live imaging was performed on the DeltaVision system. A culture dish placed on the microscope stage was covered with a chamber in which a humidified premixed gas consisting of 5% CO_2 and 95% air was infused, and the whole setup was set at 37 °C. DIC and fluorescent images were acquired at 20-min intervals. The data were processed using Softworx (Applied Precision) and, if necessary, image editing was performed using Adobe Photoshop Elements 7.0.

Semi-quantitative RT-PCR. Semi-quantitative RT-PCR was performed in standard fashion. The primer sequences used are listed in **Supplementary Table 1**. PCR products were separated on agarose gels and visualized using ImageQuant TL system (GE Healthcare).

Sorting and Hubrecht-protocol culture for single Lgr5$^+$ cells. Tamoxifen was injected into *R26R-Confetti* mice crossed with *Lgr5-EGFP-ires-CreERT2* mice, and the colonic crypts from the resulting mice were isolated 3 d later. Epithelial cells were dissociated with TrypLE express (Invitrogen) and analyzed by MoFlo (DakoCytomation). Viable single cells were gated, and then the cells doubly positive for EGFP and RFP were sorted and embedded in Matrigel (BD Bioscience) on 96-well plates. An Advanced DMEM/F12 culture medium supplemented with penicillin and streptomycin, 4-(2-hydroxyethyl)-1-piperazineethanesulfonic acid (HEPES), glutamax, N2, B27 (all from Invitrogen) and growth factors (EGF, noggin and R-spondin) was diluted 1:1 with Wnt3a-conditioned medium and used as Hubrecht medium. Y-27632 was included for the first 2 d to avoid anoikis. Growth factors were added every other day, and the entire medium was changed every 4 d. See the **Supplementary Methods** for additional details.

Transplantation experiments. For the EGFP$^+$ cell transplantations, cells isolated from colon tissues were cultured for 5 or 8 d according to the TMDU protocol and used as donor cells. For single Lgr5$^+$-cell–derived organoid transplantation, cells were expanded based on the Hubrecht protocol and then cryopreserved. The cells were then shipped, thawed and further cultured. Acute colitis was induced by feeding 6-week-old *Rag2*$^{-/-}$ mice with 3.0% DSS (molecular weight 10,000; Ensuiko Sugar Refining Co.) dissolved in drinking water for 5 d (days 1–5). At 7 and 10 d after the start of DSS administration, donor cells equivalent to those from ~500 organoids were instilled into colonic lumen as a suspension. After infusion, the anal verge was glued for 6 h. After the transplantation on day 10, mice were maintained as usual before they were killed and analyzed. See the **Supplementary Methods** for additional details.

TRITC-dextran permeability assay. Intestinal permeability was assessed by enteral administration of TRITC-dextran (molecular mass 4.4 kDa; Sigma). Transplanted or sham-transplanted mice were gavaged with TRITC-dextran 4 h before killing on day 38. Whole blood was obtained at the time of killing, and then the colonic tissues were examined for whether the EGFP$^+$ engrafts were present. TRITC-dextran measurements were performed on an ARVO MX (PerkinElmer), with serial dilutions of TRITC-dextran used as a standard curve.

Statistical analyses. Data are shown as means ± s.e.m. Data for **Figures 3f**, **4d** and **Supplementary Figure 7b** were statistically analyzed by the two-sample Student's *t* test. The data for **Supplementary Figure 5** showed non-normal distributions and were analyzed by Mann-Whitney *U* test. Statistical significance for comparisons was assigned at $P < 0.05$.

Additional methods. Detailed methodology is described in the **Supplementary Methods**.

Biochemical and Biophysical Research Communications xxx (2012) xxx–xxx

Contents lists available at SciVerse ScienceDirect

Biochemical and Biophysical Research Communications

journal homepage: www.elsevier.com/locate/ybbrc

Real-time analysis of P-glycoprotein-mediated drug transport across primary intestinal epithelium three-dimensionally cultured *in vitro*

Tomohiro Mizutani [a,1], Tetsuya Nakamura [b,*,1], Ryo Morikawa [a], Masayoshi Fukuda [a], Wakana Mochizuki [a], Yuhki Yamauchi [a], Kengo Nozaki [a], Shiro Yui [a], Yasuhiro Nemoto [a], Takashi Nagaishi [a], Ryuichi Okamoto [b], Kiichiro Tsuchiya [a], Mamoru Watanabe [a]

[a] *Department of Gastroenterology and Hepatology, Graduate School, Tokyo Medical and Dental University, 1-5-45 Yushima, Bunkyo-ku, Tokyo 113-8519, Japan*
[b] *Department of Advanced Therapeutics for GI Diseases, Graduate School, Tokyo Medical and Dental University, 1-5-45 Yushima, Bunkyo-ku, Tokyo 113-8519, Japan*

ARTICLE INFO

Article history:
Received 30 January 2012
Available online xxxx

Keywords:
P-glycoprotein
Drug transport
Intestinal absorption
Cell membrane permeability
Primary culture
Live imaging

ABSTRACT

P-glycoprotein (P-gp) is an efflux transporter that regulates bioavailability of orally administered drugs at the intestinal epithelium. To develop an *in vitro* experimental model that mimics P-gp-mediated intestinal drug transport *in vivo*, we employed normal intestinal epithelium three-dimensionally cultured. Physiological expression of P-gp mRNA and the expression of its protein at the apical membrane were observed in the small intestinal epithelium grown as cystic organoids. Rhodamine123 (Rh123), a substrate for P-gp, was actively transported in the basoapical direction and accumulated in the luminal space, while the epithelial integrity was kept intact. Furthermore, we were able to monitor the whole process of Rh123 transport and its inhibition by verapamil in real-time, from which kinetic parameters for Rh123 transport could be estimated by a mathematical modeling. The method here described to evaluate the dynamics of P-gp-mediated transport in primary intestinal epithelial cells would be instrumental in investigating the physiological function of P-gp and its inhibitors/inducers *in vitro*.

1. Introduction

Bioavailability of many clinically relevant drugs is modulated by the activity of efflux transporters expressed in the epithelial lining of the intestine [1,2]. P-glycoprotein (P-gp, also known as ABCB1), a member of the ATP-binding cassette family of transporters, is located in the apical membrane of intestinal epithelial cells [3,4] and serves as an important determinant of the disposition of many orally administered drugs [5–9]. There is, thus, a considerable interest in predicting the P-gp-mediated elimination of drug candidates and assessing the drug-drug interactions involving P-gp substrates and inhibitors/inducers in the intestinal epithelium.

Various model systems have been reported to assess the intestinal epithelial drug transport *in vitro*. Among these, cell based assays using human tumor-derived cell lines, such as Caco-2 cells, are the most commonly used method in many laboratories [10]. When grown on a membrane placed between two chambers, those cells form a well-polarized monolayer joined by tight junctions, providing a selective barrier that can be used to study influx (from the apical to the basal) and efflux (from the basal to the apical) transport of P-gp substrates [11–14]. Although such cell based systems have been well characterized and used as standard assays, several factors, such as variable expression of P-gp in those immortalized cell lines, are known to cause inter-experimental variability of the data [15,16]. Therefore, it would be of importance to develop an experimental model in which drug transport can be assessed in a reliable manner relevant to the physiological *in vivo* function of intestinal epithelium.

Recently, the long-awaited method for *in vitro* culture of normal intestinal epithelium has been developed [17]. When isolated and placed three-dimensionally, the intestinal crypts keep proliferating, forming enclosed structures with their upper openings closed. These "organoids" are lined by an epithelial monolayer containing both immature cells and terminally differentiated cells, with their apical membranes facing the luminal space inside. In light of this, we were particularly interested in determining whether this newly developed culture technology could be adapted for use in drug transport analysis.

In the present study, by developing a real-time imaging system and its mathematical modeling, we show that the primary culture of small intestinal epithelium would serve as an efficient tool to evaluate the dynamics of P-gp-mediated drug transport.

* Corresponding author. Fax: +81 3 5803 0268.
E-mail address: nakamura.gast@tmd.ac.jp (T. Nakamura).
[1] These authors contributed equally.

0006-291X/$ - see front matter © 2012 Elsevier Inc. All rights reserved.
doi:10.1016/j.bbrc.2012.01.155

Please cite this article in press as: T. Mizutani et al., Real-time analysis of P-glycoprotein-mediated drug transport across primary intestinal epithelium three-dimensionally cultured *in vitro*, Biochem. Biophys. Res. Commun. (2012), doi:10.1016/j.bbrc.2012.01.155

2. Materials and methods

2.1. 3D culture of intestinal epithelium

Culture of intestinal epithelium was performed as described previously [17]. Crypts of proximal small intestine were obtained from adult C57BL/6 mice and purified. They were counted and embedded in Matrigel (BD Biosciences) at 10,000 crypts/ml. For conventional culture, 30 μl of Matrigel was seeded on 24-well plates. For live imaging experiments, 60 μl of Matrigel was placed on 40-mm coverslips placed in 60-mm culture dishes. After the Matrigel solidified, advanced DMEM/F12 medium (Invitrogen) containing 20 ng/ml EGF (Peprotech), 100 ng/ml Noggin, 500 ng/ml R-spondin1 (R&D systems), 2 mM L-glutamine (GIBCO) and penicillin/streptomycin was overlaid. The medium was changed every 4 days. When necessary, Rh123, FITC-dextran, or verapamil (Sigma–Aldrich) was added to the medium as indicated. Animal experiments were performed with the approval of the Institutional Animal Care and Use Committee of Tokyo Medical and Dental University.

2.2. Semi-quantitative RT-PCR

Organoids were isolated from the Matrigel using BD Cell recovery solution as instructed by the manufacturer. Total RNA was isolated and 300 ng was used for cDNA synthesis in a 21 μl of reaction. 1 μl of cDNA was amplified by PCR in a 25 μl reaction. Sense (S) and antisense (AS) primers, and the cycle numbers for the amplification of each gene were as follows: S: 5'-TGCTGTGATTTTCCAGAACA-3' and AS: 5'-TCCAACATATTCGGCTTTAG-3' for Abcb1a (22 cycles); and S: 5'-CTGGCCAAGGTCATCCATGA-3' and AS: 5'-GCCATGAGGTCCACCACCCTG-3' for Gapdh (19 cycles). PCR products were separated on agarose gels and visualized using Image Quant TL system (GE Healthcare).

2.3. Immunohistochemistry

Tissues and organoids were fixed, dehydrated in 20% sucrose/PBS, and frozen in OCT compound (Tissue Tek). Cryosections (6 μm thick) were immunostained with an anti-Mdr antibody (1 μg/ml, Santa Cruz Biotechnology) and a fluorescent secondary antibody (Alexa Fluor 588, Molecular Probes). The sections were also counterstained with DAPI (Vector Laboratories) to visualize nuclei. Images were acquired on a fluorescence microscope DeltaVision system (Applied Precision).

2.4. Live imaging

The isolated crypts were mixed with Matrigel and placed on 40-mm glass coverslips so that the whole gel would be as thin as possible (<1 mm). On Day 3, the coverslip was incorporated into the FCS-2 closed cell chamber (Bioptechs), the thickness of which was set at 1 mm. The chamber was fixed on the stage of a DeltaVision microscope system covered with a thermally-controlled enclosure set at 37 °C. Spherical organoids with diameters of around 50 μm were chosen and imaged using a fluorescent microscope IX-71 (Olympus) equipped with a xenon light source, a UplansApo 10x objective (0.4 numerical aperture), a 490/20-nm excitation filter, a 528/38-nm filter, and a Cool Snap ES2 digital camera (Roper Scientific). Differential interference contrast (DIC) and fluorescent images were acquired at 3 min intervals. Exposure times were 0.2 s for DIC and 0.03 s for fluorescent images, respectively, with 1 × 1 binning and an image size of 512 × 512 pixels. These conditions were kept throughout all experiments. Immediately after the third time frame of imaging (6 min after the start), 5 ml of pre-warmed medium containing Rh123 (1 μM), with or without various concentration of verapamil, was rapidly infused from one port on the side of the chamber, allowing the preexisting medium inside to direct out of the chamber from the other side. This enabled a rapid replenishment of medium with no disturbance of the position or morphology of the organoids. All experiments were performed for 5 h and 30 min.

2.5. Data analysis and mathematical modeling

Images at individual time points of all organoids were quantitatively assessed using the SoftWoRx (Applied Precision). For individual images, circular areas with a diameter of 30 μm were manually set inside (luminal space) and outside (culture medium) of the organoid, and the fluorescent signal for each compartment was expressed by average pixel values of the circular area. The outer intensities (culture medium) of the images acquired immediately before (0 μM) and after (1 μM) the Rh123 addition were applied for calculating the concentration of all other areas of a given experiment.

For mathematical modeling, we made an assumption that Rh123 concentration in the lumen is determined only by active inward transport and passive bidirectional diffusion, both of which take place at the inner apical membrane. When Rh123 concentration (1 μM) remains stable in the donor side due to the excessively large volume in space, the rate of active transport in the basal to apical direction, V_{in} (nmol/s), can be expressed as below:

$$V_{in} = P_{app.active} \cdot S \cdot C_{out} \tag{1}$$

In this equation (Eq. (1)), $P_{app.active}$ (cm/s) is the apparent permeability coefficient of active basoapical transport, S (cm^2) is the area of inner surface of the organoids, and C_{out} (μmol/litter; nmol/cm^3) is the outer concentration of Rh123 given as 1. Passive diffusion of Rh123 can occur in both directions, depending on the concentration gradient across the apical membrane. When V_{out} (nmol/s) is defined as the rate of diffusion in the apical to basal direction, it is derived from an equation,

$$V_{out} = P_{app.passive} \cdot S \cdot (C_{in}(t) - C_{out}) \tag{2}$$

where $P_{app.passive}$ (cm/s) is the apparent permeability coefficient of bidirectional passive diffusion, S (cm^2) is the inner surface area, and C_{in} (nmol/cm^3) is the luminal Rh123 concentration that can be defined as a function of time t. The total amounts of Rh123, transported across the apical membrane inward and outward by a given time t, can be expressed as integral functions $Q_{in}(t)$ and $Q_{out}(t)$, respectively.

$$Q_{in}(t) = \int_0^t V_{in} dt = V_{in} \cdot t \tag{3}$$

$$Q_{out}(t) = \int_0^t V_{out} dt \tag{4}$$

Eq. (1) and (2) can be substituted into Eq. (3) and (4), respectively, to convert equations as below:

$$Q_{in}(t) = P_{app.active} \cdot S \cdot C_{out} \cdot t \tag{5}$$

$$Q_{out}(t) = P_{app.passive} \cdot S \cdot \int_0^t C_{in}(t) dt - P_{app.passive} \cdot S \cdot C_{out} \cdot t \tag{6}$$

The luminal spatial volume, Vol (cm^3), can be assumed to stay unchanged during the imaging and, thus, C_{in} (t) can also be expressed as below:

$$C_{in}(t) = \frac{Q_{in}(t) - Q_{out}(t)}{Vol} \tag{7}$$

From Eq. (5)–(7), C_{in} (t) can now be solved as a function of the variable t.

Please cite this article in press as: T. Mizutani et al., Real-time analysis of P-glycoprotein-mediated drug transport across primary intestinal epithelium three-dimensionally cultured *in vitro*, Biochem. Biophys. Res. Commun. (2012), doi:10.1016/j.bbrc.2012.01.155

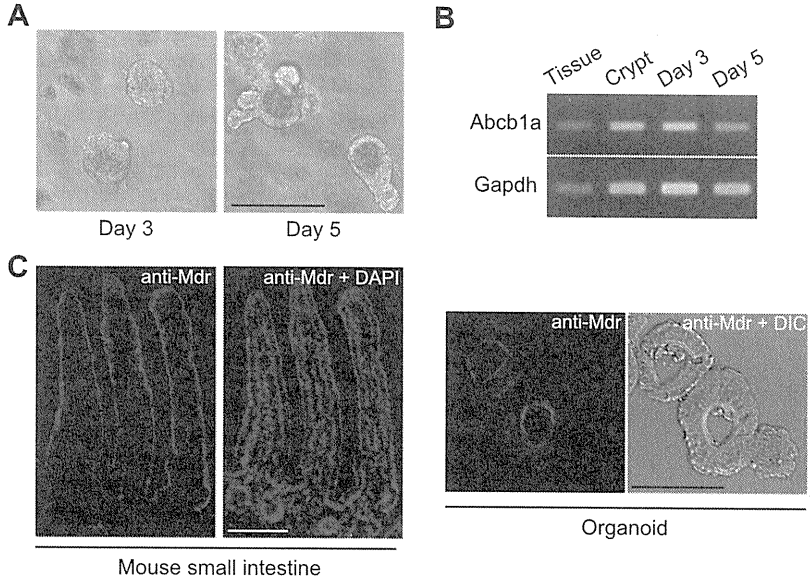

Fig. 1. Physiological expression of P-gp in cultured small intestinal organoids. (A) Phase contrast images of small intestinal organoids on Day 3 (left) and Day 5 (right) of culture. Scale bar, 100 μm. (B) Expression of P-gp (*Abcb1a*) mRNA analyzed by semi-quantitative RT-PCR. Expression levels in the whole small intestine (tissue), isolated crypts (crypt), and the organoids on Day 3 and Day 5 are shown (top). PCR products for *Gapdh* are shown as internal controls (bottom). (C) Localization of P-gp proteins. Immunohistochemistry with an anti-Mdr antibody was performed for mouse proximal small intestine tissue (mouse small intestine) and cultured organoids on Day 3 (organoid). Scale bars, 100 μm.

$$C_{in}(t) = \frac{P_{app.active} + P_{app.passive}}{P_{app.passive}} \cdot C_{out} + e^{-P_{app.passive} \cdot \frac{S}{Vol} t} \cdot \left(C_{in}(0) - \frac{P_{app.active} + P_{app.passive}}{P_{app.passive}} \cdot C_{out} \right) \quad (8)$$

The inner Rh123 concentrations calculated from the fluorescent intensities of each experiment were plotted and then fitted to the function characterized in Eq. (8) using curve fitting on MATLAB software (The MathWorks, Inc.). By applying this process to the dataset obtained from each organoid, we could retrieve two kinetic parameters A (nmol/cm^3) and B (s^{-1}) as indicated below:

$$A = \frac{P_{app.acitve} + P_{app.passive}}{P_{app.passive}} \cdot C_{out} \quad (9)$$

$$B = P_{app.passive} \cdot \frac{S}{Vol} \quad (10)$$

Substituting $4\pi r^2$ and $4\pi r^3/3$ (r denotes the radius of organoid) into S and Vol, respectively, $P_{app.active}$ and $P_{app.passive}$ could be finally determined as below:

$$P_{app.passive} = \frac{B \cdot r}{3} \quad (11)$$

$$P_{app.active} = \frac{A - C_{out}}{C_{out}} \cdot P_{app.passive} = \frac{r}{3} \cdot B \cdot \frac{A - C_{out}}{C_{out}} \quad (12)$$

2.6. Statistical analysis

Data were presented as means ± s.e. Statistical analysis was performed using the Student's t-test or Welch's t-test (Fig. 4C). Statistical significance for comparisons was assigned at $P < 0.01$ (Fig. 4C).

3. Results

First we assessed the expression of P-gp in intestinal epithelium obtained from murine small intestine and three-dimensionally cultured. As previously described [17], they grew as epithelial organoids showing round cystic structures on Day 3, and then formed asymmetric structures having growing crypt-like protrusions on Day 5 (Fig. 1A). In the mouse, P-gp is encoded by two genes, Abcb1a and Abcb1b. We could detect the expression of Abcb1a in the intestinal tissue by our semi-quantitative RT-PCR (Fig. 1B), while Abcb1b mRNA was hardly detectable even with a high number of amplification cycles (data not shown). This supported the previous finding that Abcb1a is the major species of P-gp expressed in the small intestine [18]. In the cultured organoids, expression of Abcb1a stayed unchanged on Day 3 compared with that of isolated crypts on Day 1, whereas a slight decrease in its expression was noted on Day 5 (Fig. 1B). We also tested the expression of P-gp protein. Immunostaining with an antibody,

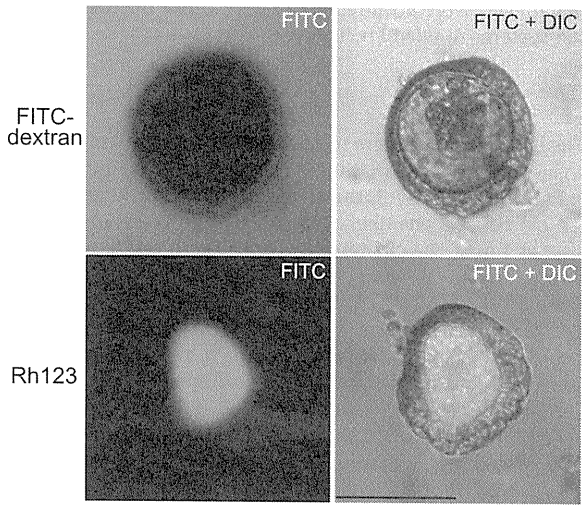

Fig. 2. Cultured organoids actively transport Rh123, while keeping their epithelial integrity. FITC-dextran (2mM, top) or Rh123 (1 μM, bottom) was added to the culture medium on Day 3, and images were acquired 5 h after the addition of the fluorescent probes. Fluorescent images (FITC) and their merged ones with DIC (FITC + DIC) are shown. Scale bar, 100 μm.

Please cite this article in press as: T. Mizutani et al., Real-time analysis of P-glycoprotein-mediated drug transport across primary intestinal epithelium three-dimensionally cultured *in vitro*, Biochem. Biophys. Res. Commun. (2012), doi:10.1016/j.bbrc.2012.01.155

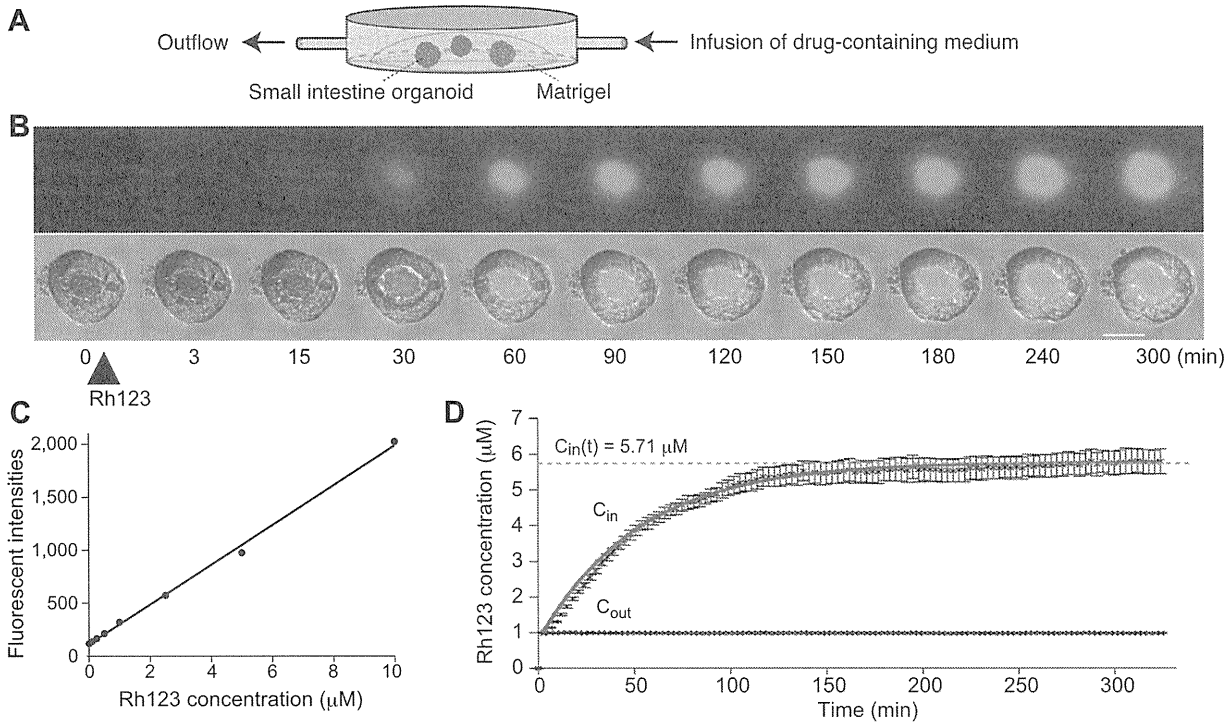

Fig. 3. Dynamics of Rh123 transport by cultured organoids and its mathematical modeling. (A) A schematic representation of the closed perfusable micro-observation chamber used for the time-lapse imaging. (B) Still images from time series of a Day 3 organoid actively transporting Rh123. Time 0 denotes the time frame immediately before the perfusion of Rh123. Fluorescent (FITC) images and their merged ones with DIC (FITC + DIC) are shown. Scale bar, 50 μm. The whole images can be viewed as Supplementary Video 1. (C) The linear correlation between the fluorescent intensity (expressed in arbitrary units) and Rh123 concentration under cell-free condition of the same experimental setting. (D) Rh123 concentrations inside and outside of organoids were calculated from data obtained by time-lapse experiments and plotted as mean ± s.e. (n = 10). A curve obtained by fitting a mathematical model to data is shown in red. (For interpretation of the references to colour in this figure legend, the reader is referred to the web version of this article.)

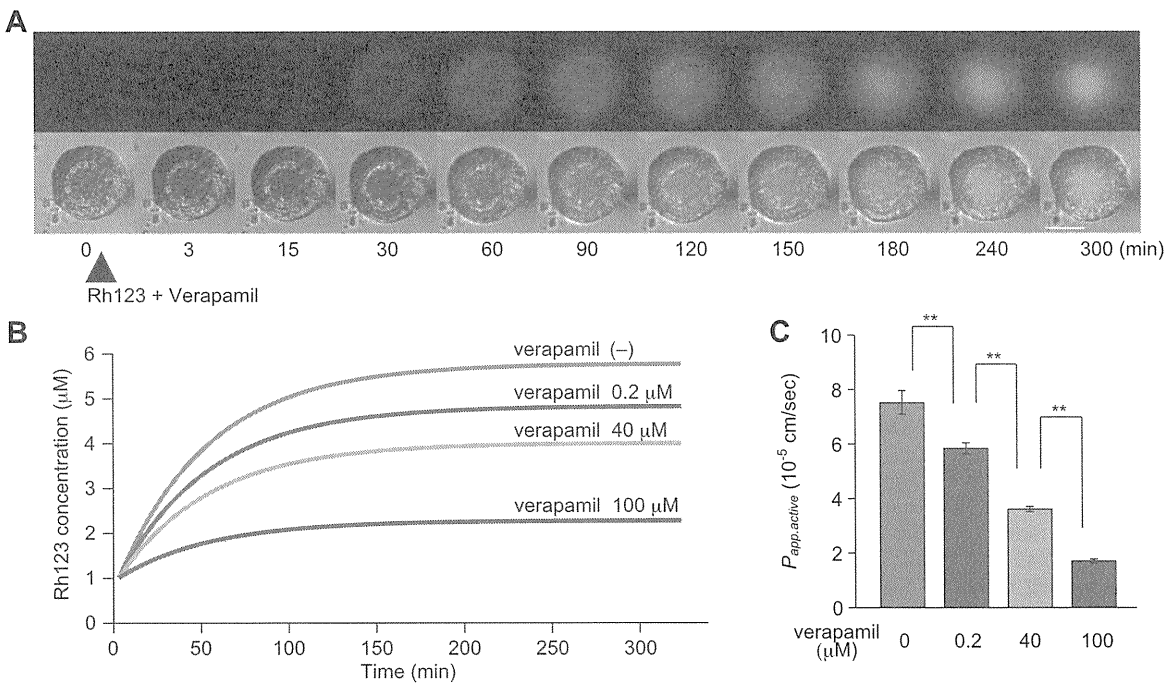

Fig. 4. Verapamil inhibits Rh123 transport across primary intestinal epithelium. (A) Time-lapse imaging experiments were performed as described in Fig. 3 in the presence of 40 μM verapamil. Fluorescent (FITC) and merged (FITC + DIC) images of a representative movie are shown. Scale bar, 50 μm. The video including these data, and other videos of the representative organoids recorded in the presence of 0.2 and 100 μM verapamil can be viewed as Supplementary Videos 2–4. (B) The curves obtained by fitting the mathematical model to data of verapamil inhibition experiments. (C) The $P_{app.active}$ values at various doses of verapamil were calculated and shown as mean ± s.e. (n = 10 for each) $^{**}P < 0.01$.

Please cite this article in press as: T. Mizutani et al., Real-time analysis of P-glycoprotein-mediated drug transport across primary intestinal epithelium three-dimensionally cultured *in vitro*, Biochem. Biophys. Res. Commun. (2012), doi:10.1016/j.bbrc.2012.01.155

capable of labeling Abcb1a on the apical surface of epithelium in the small intestinal tissue (Fig. 1C), revealed predominant expression of the transporter on the inner surface of cultured organoids on Day 3 (Fig. 1C). These results showed that the intestinal epithelial cells maintain physiological expression level and correct localization of P-gp in primary culture.

When the medium was supplemented with FITC-dextran of 4 kDa on Day 3 of culture, its fluorescent signals were excluded from the lumen even at 5 h after the supplementation (Fig. 2, top). This indicated the preservation of epithelial integrity not allowing paracellular flux of this well-characterized permeability probe. Meanwhile, Rh123, a fluorescent dye known as a substrate of P-gp [13,19,20], showed a different behavior. Its intense fluorescent signals were observed in the lumen 5 h after the addition with a stark contrast against those in outer space of organoids (Fig. 2, bottom). This clearly showed that the intestinal organoids in culture are able to conduct active transepithelial transport of Rh123 in the basal to apical direction, and the involvement of P-gp in this process was strongly suggested.

To assess the dynamics of basoapical transport of Rh123, we developed an experimental system where the whole process could be visualized in real-time (Fig. 3A). On Day 3 of culture, the organoids were placed in a micro-observation chamber having a perfusable space inside, and the ones having spherical structures with diameters of around 50 μm were chosen for imaging. The time-lapse imaging at 3 min intervals was initiated, and then the whole culture medium was replaced with Rh123 (1 μM)-containing medium immediately after the image acquisition of the third time frame (referred to as time 0 hereafter).

The fluorescent intensity of the area outside of organoids rose by the first time frame after the perfusion (3 min), indicating the rapid diffusion of Rh123 throughout the optical chamber (Fig. 3B). The luminal signals were at a comparable level to the outer signals by this time point, and then rapidly went up far exceeding the signals outside. Thereafter, this upward trend gradually declined and the enrichment of Rh123 in the inner space appeared to approach a steady-state level (Fig. 3B, Supplementary Video 1). Based on the finding that the measured fluorescent intensity was linearly correlated with Rh123 concentration under the cell-free condition of the same experimental setting (Fig. 3C), we could calculate both inner and outer concentrations of Rh123 at individual time frames for all organoids (Fig. 3D). Rh123 concentration outside stayed nearly constant, assumably because the large excess of outer spatial volume made the loss of Rh123 into the lumen almost negligible (Fig. 3D).

In order to obtain several kinetic parameters of Rh123 transport, we constructed a mathematical model on the assumption that Rh123 concentration in the tightly-closed lumen was determined only by two mechanisms at the apical cell membrane: active inward transport and passive bidirectional diffusion (See Section 2). Analysis of the dataset ($n = 10$) by the mathematical function based on this simplified two-compartment model provided a well-fitted curve (Fig. 3D, red). From this, we could extract two parameters as defined in Materials and Methods (Eq. (9) and (10)). As a result, when the observed organoids were all assumed to be spheres with a radius of 25 μm, $P_{app.active}$ and $P_{app.passive}$ were calculated as $7.53 \pm 0.45 \times 10^{-5}$ cm/s and $1.63 \pm 0.08 \times 10^{-5}$ cm/s, respectively, according to Eq. (11) and (12). Importantly, given the Eq. (8), the limit of function $C_{in}(t)$ (as t approaches infinity) could be expressed as follows:

$$\lim_{t\to\infty} C_{in}(t) = \frac{P_{app.active} + P_{app.passive}}{P_{app.passive}} \cdot C_{out} \tag{13}$$

Indeed, when $P_{app.active}$ and $P_{app.passive}$ were substituted with the values described above and C_{out} was regarded as a constant value of 1 μM, the obtained limit value of 5.71 μM represented the concentration toward which the observed C_{in} was approaching (Fig. 3D). In addition, using this model with data analysis, the ratio of basoapical active transport and bidirectional passive diffusion, $P_{app.active}/P_{app.passive}$, could be determined as around 4.6-fold, independently of the radius of organoids, r.

To assess the involvement of P-gp in Rh123 transport, we also performed time-lapse experiments where Rh123 was infused together with different doses (0.2, 40 and 100 μM) of verapamil, an inhibitor for P-gp [11,12,19]. The initial rate of transport as well as the steady-state level of the luminal Rh123 in later phases was obviously suppressed in the presence of verapamil at each dose (Fig. 4A, Supplementary Videos 2–4). According to a simple assumption that verapamil would not affect $P_{app.passive}$, we could obtain the fitting curves (Fig. 4B) by mathematical modeling of the data ($n = 10$ for each dose of verapamil), which again allowed quantitative estimates for kinetic parameters. The derived $P_{app.active}$ indicated that 40 μM of verapamil had ~50% inhibitory effect on Rh123 transport under this experimental condition (Fig. 4C).

4. Discussion

In this study, we have developed an experimental system to investigate P-gp-mediated drug transport across the small intestinal epithelium in primary culture. To date, many attempts have been made to assess the permeability of normal intestine *in vitro* including the use of excised intestinal tissues with or without the underlying submucosal layers. However, the common disadvantage of such approach has been the limited viability of intestinal tissues when isolated [16]. By contrast, as represented by Caco-2 cells, immortal cell lines have been extensively used, partly due to the ease with which the cells can be cultured. Many studies have shown the correlation between *in vitro* permeability values in Caco-2 assays and parameters of *in vivo* absorption [21–24]. However, it is pointed out that variability of the results may exist across experiments, due to the heterogeneity of the cells resulting from the phenotypic drift during the culture under different conditions. In this regard, the most distinctive feature of our system is the use of purified, non-transformed intestinal epithelial cells keeping their physiological expression and localization of P-gp. We also showed that Rh123 transport was inhibited by verapamil, indicating the functional involvement of P-gp in this process. Such availability of primary intestinal epithelium for transport assays would build a basis for a variety of application including the screening of inducers/inhibitors of P-gp in normal intestinal cells, or assessing the P-gp function in individual human specimens.

Another key feature of the presented method is its simple and rapid procedure. In the Caco-2 cell system, drugs are added to one side of the cell layer and their appearance in the other side is quantitatively measured. Experiments to calculate permeability in both directions are needed, and then P-gp-mediated transport is suggested when a higher basoapical permeability is observed [11–13]. On the other hand, even with a simple unidirectional assessment, spatial characteristics of the organoids in the present system, having tightly closed space inside, provided an intuitive information as to whether the net rate of inward transport exceeds that of outward diffusion by the luminal accumulation of fluorescence. In addition, taking advantage of time-lapse imaging and mathematical modeling, we could quantitatively estimate the ratio of basoapical active transport and bidirectional passive diffusion ($P_{app.active}/P_{app.passive}$). From Eq. (13), this ratio can also be expressed as below:

$$\frac{P_{app.active}}{P_{app.passive}} = \frac{\lim_{t\to\infty} C_{in}(t)}{C_{out}} - 1 \tag{14}$$

Please cite this article in press as: T. Mizutani et al., Real-time analysis of P-glycoprotein-mediated drug transport across primary intestinal epithelium three-dimensionally cultured *in vitro*, Biochem. Biophys. Res. Commun. (2012), doi:10.1016/j.bbrc.2012.01.155

This further indicates that the parameter $P_{app.active}/P_{app.passive}$ would be simply estimated when the ratio of inner versus outer drug concentration at an equilibrium state is obtained.

In conclusion, we have described a simple, rapid and efficient method to evaluate the dynamics of P-gp-mediated transport in normal intestinal epithelium *in vitro*. This system would be instrumental in investigating the physiological function and screening of inhibitors/inducers of P-gp and, thus, serve as a novel tool to study the bioavailability of drugs via the intestinal epithelium.

Acknowledgments

We sincerely thank Marc-Aurele Brun for his help and contribution to mathematical modeling and curve fit analysis. This study was supported by Grant-in-Aid for Scientific Research from the Japanese Ministry of Education, Culture, Sports, Science and Technology, and by Health and Labor Sciences Research Grants for Research on Intractable Diseases from the Ministry of Health, Labor and Welfare of Japan.

Appendix A. Supplementary data

Supplementary data associated with this article can be found, in the online version, at doi:10.1016/j.bbrc.2012.01.155.

References

[1] M. Takano, R. Yumoto, T. Murakami, Expression and function of efflux drug transporters in the intestine, Pharmacol. Ther. 109 (2006) 137–161.
[2] J.R. Kunta, P.J. Sinko, Intestinal drug transporters: in vivo function and clinical importance, Curr. Drug. Metab. 5 (2004) 109–124.
[3] F. Thiebaut, T. Tsuruo, H. Hamada, M.M. Gottesman, I. Pastan, M.C. Willingham, Cellular localization of the multidrug-resistance gene product P-glycoprotein in normal human tissues, Proc. Natl. Acad. Sci. USA 84 (1987) 7735–7738.
[4] S. Hsing, Z. Gatmaitan, I.M. Arias, The function of Gp170, the multidrug-resistance gene product, in the brush border of rat intestinal mucosa, Gastroenterology 102 (1992) 879–885.
[5] M.F. Fromm, P-glycoprotein: a defense mechanism limiting oral bioavailability and CNS accumulation of drugs, Int. J. Clin. Pharmacol. Ther. 38 (2000) 69–74.
[6] R.B. Kim, M.F. Fromm, C. Wandel, B. Leake, A.J. Wood, D.M. Roden, G.R. Wilkinson, The drug transporter P-glycoprotein limits oral absorption and brain entry of HIV-1 protease inhibitors, J. Clin. Invest. 101 (1998) 289–294.
[7] G.Y. Kwei, R.F. Alvaro, Q. Chen, H.J. Jenkins, C.E. Hop, C.A. Keohane, V.T. Ly, J.R. Strauss, R.W. Wang, Z. Wang, T.R. Pippert, D.R. Umbenhauer, Disposition of ivermectin and cyclosporin A in CF-1 mice deficient in mdr1a P-glycoprotein, Drug Metab. Dispos. 27 (1999) 581–587.
[8] A. Sparreboom, J. van Asperen, U. Mayer, A.H. Schinkel, J.W. Smit, D.K. Meijer, P. Borst, W.J. Nooijen, J.H. Beijnen, O. van Tellingen, Limited oral bioavailability and active epithelial excretion of paclitaxel (Taxol) caused by P-glycoprotein in the intestine, Proc. Natl. Acad. Sci. USA 94 (1997) 2031–2035.
[9] J. van Asperen, O. van Tellingen, J.H. Beijnen, The role of mdr1a P-glycoprotein in the biliary and intestinal secretion of doxorubicin and vinblastine in mice, Drug Metab. Dispos. 28 (2000) 264–267.
[10] I.J. Hidalgo, T.J. Raub, R.T. Borchardt, Characterization of the human colon carcinoma cell line (Caco-2) as a model system for intestinal epithelial permeability, Gastroenterology 96 (1989) 736–749.
[11] J. Hunter, M.A. Jepson, T. Tsuruo, N.L. Simmons, B.H. Hirst, Functional expression of P-glycoprotein in apical membranes of human intestinal Caco-2 cells. Kinetics of vinblastine secretion and interaction with modulators, J. Biol. Chem. 268 (1993) 14991–14997.
[12] R. Yumoto, T. Murakami, Y. Nakamoto, R. Hasegawa, J. Nagai, M. Takano, Transport of rhodamine 123, a P-glycoprotein substrate, across rat intestine and Caco-2 cell monolayers in the presence of cytochrome P-450 3A-related compounds, J. Pharmacol. Exp. Ther. 289 (1999) 149–155.
[13] M. Takano, R. Hasegawa, T. Fukuda, R. Yumoto, J. Nagai, T. Murakami, Interaction with P-glycoprotein and transport of erythromycin, midazolam and ketoconazole in Caco-2 cells, Eur. J. Pharmacol. 358 (1998) 289–294.
[14] J.M. Dintaman, J.A. Silverman, Inhibition of P-glycoprotein by D-alpha-tocopheryl polyethylene glycol succinate (TPGS), Pharm. Res. 16 (1999) 1550–1556.
[15] H. van De Waterbeemd, D.A. Smith, K. Beaumont, D.K. Walker, Property-based design: optimization of drug absorption and pharmacokinetics, J. Med. Chem. 44 (2001) 1313–1333.
[16] I.J. Hidalgo, Assessing the absorption of new pharmaceuticals, Curr. Top. Med. Chem. 1 (2001) 385–401.
[17] T. Sato, R.G. Vries, H.J. Snippert, M. van de Wetering, N. Barker, D.E. Stange, J.H. van Es, A. Abo, P. Kujala, P.J. Peters, H. Clevers, Single Lgr5 stem cells build crypt-villus structures in vitro without a mesenchymal niche, Nature 459 (2009) 262–265.
[18] J.M. Croop, M. Raymond, D. Haber, A. Devault, R.J. Arceci, P. Gros, D.E. Housman, The three mouse multidrug resistance (mdr) genes are expressed in a tissue-specific manner in normal mouse tissues, Mol. Cell Biol. 9 (1989) 1346–1350.
[19] M.D. Perloff, E. Stormer, L.L. von Moltke, D.J. Greenblatt, Rapid assessment of P-glycoprotein inhibition and induction in vitro, Pharm. Res. 20 (2003) 1177–1183.
[20] J.S. Lee, K. Paull, M. Alvarez, C. Hose, A. Monks, M. Grever, A.T. Fojo, S.E. Bates, Rhodamine efflux patterns predict P-glycoprotein substrates in the National Cancer Institute drug screen, Mol. Pharmacol. 46 (1994) 627–638.
[21] P. Artursson, J. Karlsson, Correlation between oral drug absorption in humans and apparent drug permeability coefficients in human intestinal epithelial (Caco-2) cells, Biochem. Biophys. Res. Commun. 175 (1991) 880–885.
[22] D.C. Kim, P.S. Burton, R.T. Borchardt, A correlation between the permeability characteristics of a series of peptides using an in vitro cell culture model (Caco-2) and those using an in situ perfused rat ileum model of the intestinal mucosa, Pharm. Res. 10 (1993) 1710–1714.
[23] M.D. Ribadeneira, B.J. Aungst, C.J. Eyermann, S.M. Huang, Effects of structural modifications on the intestinal permeability of angiotensin II receptor antagonists and the correlation of in vitro, in situ, and in vivo absorption, Pharm. Res. 13 (1996) 227–233.
[24] B.H. Stewart, O.H. Chan, R.H. Lu, E.L. Reyner, H.L. Schmid, H.W. Hamilton, B.A. Steinbaugh, M.D. Taylor, Comparison of intestinal permeabilities determined in multiple in vitro and in situ models: relationship to absorption in humans, Pharm. Res. 12 (1995) 693–699.

Please cite this article in press as: T. Mizutani et al., Real-time analysis of P-glycoprotein-mediated drug transport across primary intestinal epithelium three-dimensionally cultured *in vitro*, Biochem. Biophys. Res. Commun. (2012), doi:10.1016/j.bbrc.2012.01.155

Luminal CD4+ T Cells Penetrate Gut Epithelial Monolayers and Egress From Lamina Propria to Blood Circulation

YASUHIRO NEMOTO,* TAKANORI KANAI,‡ TAMAKO SHINOHARA,* TAKASHI ITO,§ TETSUYA NAKAMURA,* RYUICHI OKAMOTO,* KIICHIRO TSUCHIYA,* MARTIN LIPP,‖ YOSHINOBU EISHI,§ and MAMORU WATANABE*

*Department of Gastroenterology and Hepatology, Graduate School, Tokyo Medical and Dental University, Tokyo; ‡Division of Gastroenterology and Hepatology, Department of Internal Medicine, Keio University School of Medicine, Tokyo; §Department of Pathology, Graduate School, Tokyo Medical and Dental University, Tokyo, Japan; and ‖Department of Tumor Genetics and Immunogenetics, Max-Delbruck Center for Molecular Medicine, Berlin, Germany

BACKGROUND & AIMS: The egress of memory T cells from peripheral tissues, such as lung and skin, into the draining lymph nodes requires their expression of CC chemokine receptor 7 (CCR7). In the intestine, resident memory T cells in the intestinal lamina propria (LP) do not express CCR7, indicating that they are tissue bound and do not exit the intestine. **METHODS:** We developed a cell transfer system, using rectal administration of lymphocytes to C57BL/6 mice. Lymphotoxin α-deficient mice were crossed with *RAG-2*$^{-/-}$ (recombination-activating gene-2) mice to generate *lymphotoxin α-deficient* × *RAG-2*$^{-/-}$ mice. **RESULTS:** Severe combined immunodeficient (SCID) or *RAG-2*$^{-/-}$ mice given rectal administration of splenic CD4+ T cells from normal mice developed colitis; the cells proliferated not only in the LP but also in spleen. SCID or *RAG-2*$^{-/-}$ mice given rectal administrations of CD4+ T cells that expressed green fluorescent protein (GFP+CD4+ T cells) localized to the LP within 6 hours but were not found in the spleen until 24 hours after administration. Immunohistochemical and electron microscopic analyses detected CD4+ T cells in the intraepithelial space just 3 hours after intrarectal administration. However, neither CCR7 deficiency nor the sphingosine-1-phosphate receptor agonist Fingolimod impaired the egress of CD4+ T cells from LP to systemic circulation. **CONCLUSIONS: CD4+ T cells not only penetrate from the luminal side of the intestine to the LP but also actively egress from the LP into the circulation. We developed a rectal administration system that might be used to further investigate cell trafficking in intestinal mucosa and to develop enema-based therapeutics for intestinal diseases.**

Keywords: T-Cell Migration; Localization; Mouse Model; Chemokine; Treatment.

BASIC AND TRANSLATIONAL AT

Although accumulated evidence has revealed how effector/memory T cells migrate to peripheral tissues, there are still many enigmas about how these cells egress from peripheral tissues to blood circulation. Egress of immune cells from nonlymphoid peripheral tissues is a critical step in lymphocyte migration as well as lymphocyte homing to these tissues.[1–4] It has been reported that the draining lymphatics of tissues contain substantial numbers of CD4+ and CD8+ lymphocytes, some of which are of memory phenotype,[5,6] but it remains unclear whether these memory lymphocytes are derived from cells that have egressed from peripheral tissues or from the blood via lymph nodes located at closer sites to peripheral tissues.

Recent reports suggest that the egress of effector or memory CD4+ and CD8+ T cells into the draining lymph nodes from the lung[7] and of B cells and naïve or memory CD4+ and CD8+ T cells into the popliteal lymph nodes from the footpad of skin[8] requires the expression of CCR7 on these cells. In the intestine, however, the unique phenotype (CCR9 or integrin $\alpha_4\beta_7$ or $\alpha_E\beta_7$-expressing cells) of the resident memory T cells and the lack of such cells elsewhere suggest that memory T cells in the intestinal lamina propria (LP) and intraepithelial space are tissue bound and do not exit the intestine,[1] but this theory remains unproven experimentally.

The intrarectal administration of cells employed in this study was suggested by the fact that intratracheal instillation of cells in mice can induce their cell migration to the lung and thereafter to the blood systemically.[6] In this paper, we demonstrate that living CD4+ T cells can not only penetrate intestinal barriers from the lumen to the LP but also constantly egress from the LP to the bloodstream constantly in a CCR7- and sphingosine 1-phosphate 1 ($S1P_1$)-independent manner.

Materials and Methods

Please see Supplementary Materials and Methods for more details.

Animals

C57BL/6 mice were purchased from Japan CLEA (Tokyo, Japan). C57BL/6-Ly5.1 and C57BL/6-RAG-2$^{-/-}$ mice were obtained from Taconic Laboratory (Hudson, NY) and Central Laboratories for Experimental Animals (Kawasaki, Japan). CCR7$^{-/-}$ mice were previously generated by M. Lipp (Max-Delbruck Cen-

Abbreviations used in this paper: BM, bone marrow; DC, dendritic cells; GFP, green fluorescent protein; LP, lamina propria; MLN, mesenteric lymph node; NK, natural killer; PB, peripheral blood; SCID, severe combined immunodeficient; SP, spleen; S1P, sphingosine 1-phosphate; T_{EM}, effector-memory T; Tg, transgenic; T_R, regulatory T; UC, ulcerative colitis; WT, wild type.

0016-5085/$36.00
doi:10.1053/j.gastro.2011.08.035

ter for Molecular Medicine, Berlin, Germany).[9] Green mice (CAG-green fluorescent protein [GFP] transgenic [Tg] mice) were originally generated by M. Okabe (Osaka University, Japan).[10] Lymphotoxin α (LT α)-deficient ($LT\alpha^{-/-}$) mice were purchased from The Jackson Laboratory (Bar Harbor, ME) and intercrossed into RAG-$2^{-/-}$ mice to generate $LT\alpha^{-/-}$ × RAG-$2^{-/-}$ mice. Mice were maintained under specific pathogen-free conditions in the Animal Care Facility of Tokyo Medical and Dental University. Donors and recipients were used at 6–12 weeks of age. All experiments were approved by the regional animal study committees and were done according to institutional guidelines and Home Office regulations.

Results

Substantial Numbers of Lymphocytes Reside in Crypt Abscesses of Inflamed Mucosa in Patients With Ulcerative Colitis

Accumulating evidence suggests an active moving state of immune compartments between intestinal epithelial cell barriers that separate the inside and outside of the body. For instance, recent reports demonstrated that murine CX3CR1+ dendritic cells (DC) beneath intestinal epithelial cells in small intestine penetrate epithelial barriers by extending dendrites into the luminal side through intraepithelial gaps to capture antigens including commensal bacteria.[11] In addition, it is well-known that large amounts of granulocytes accumulate in the crypt of inflamed mucosa of patients with human inflammatory bowel diseases, suggesting that granulocytes actively penetrate intestinal barriers into the luminal side under inflammatory conditions.[12] This accumulation is pathologically defined as a "crypt abscess," which is one feature of chronic inflammatory diseases of the intestine, such as ulcerative colitis (UC).[12] However, it remains largely unknown whether this is a case with other immune compartments, such as CD4+ T lymphocytes. We therefore re-evaluated immune cell compartments in crypt abscesses in colonic inflamed mucosa of patients with severe UC (Supplementary Table 1). As shown in Figure 1*A* and *B*, in addition to a major compartment, myeloperoxidase-positive granulocytes, we found that substantial numbers of CD4+ and CD8+ T cells and CD20+ B cells, but not CD56+ natural killer (NK) cells, reside in cell aggregates of crypt abscess, suggesting that these lymphocytes can actively commute across the intestinal epithelial barriers.

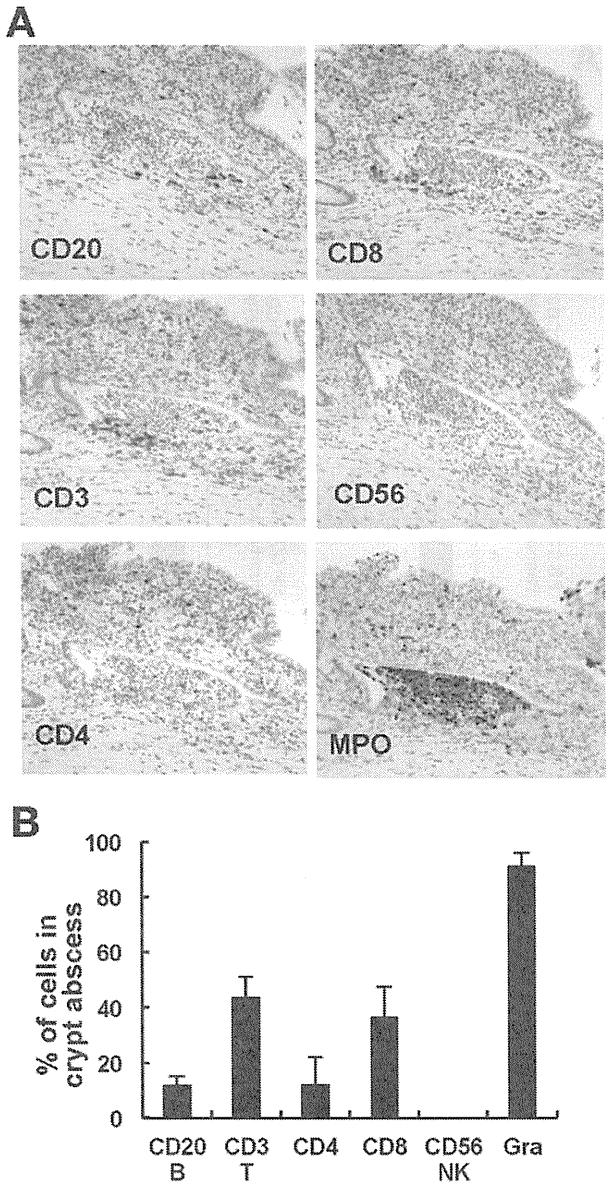

Figure 1. CD4+ T cells reside in crypt abscesses of inflamed mucosa of patients with ulcerative colitis (UC). (*A*) Immunohistochemistry of CD20, CD3, CD4, CD8, CD56, and myeloperoxidase (*MPO*) using samples of patients with severe UC. Four patients with UC (Supplementary Table 1) were examined. Sections were stained brown with a given antibody and counterstained with Mayer's hematoxylin. Representative section of crypt abscess with each stain. Original magnification, ×100. (*B*) Proportion of each compartment per total stained cell number (CD3+ + CD20+ + CD56+ + MPO+) in each crypt abscess.

SCID Mice Intrarectally Administered With Splenic CD4+ T Cells Developed Severe Colitis

Given the above results from human samples of crypt abscesses in inflamed mucosa of UC, we hypothesized that lymphocytes can actively move across intestinal epithelial barriers and therefore that intrarectally administered CD4+ T cells should, conversely, penetrate them from the lumen side. If so, this approach seems to be an ideal strategy to experimentally determine whether intestinal LP CD4+ T cells can thereafter egress LP to the systemic circulation. However, because a huge number of intestinal bacteria, over 10^3 million per mouse constantly occupy the intestinal lumen,[13–15] no attempts to intrarectally administer the cells have yet been reported. To test our hypothesis, we administered splenic CD4+ T cells from normal BALB/c mice intrarectally or intraperitoneally (as a control) into C.B-17 SCID mice (Figure 2*A*). This adoptive transfer system into immunodeficient recipients was adopted because it can be easily assessed whether intrarectally administered cells can penetrate intestinal barriers to the LP by amplifying the cell number of pen-